Impact of $Cr^{3+}/Mo^{6+}/W^{6+}$ doping on dipolar relaxation and AC conductivity in Li_2O-Al_2O_3-SiO_2 glasses

Seetepalli Vijaya krishna[a], Luka Pavić[b*], Arijeta Bafti[c], Jana Pisk[d], Dhanisetti Bhadrarao[a], Yeti Dana Rao[a], Ayyagari Venkata Sekhar[a,e], Vandana Chitti Babu[f], Vandana Ravi Kumar[a*], Nalluri Veeraiah[a,g,*]

[a]Department of Physics, Acharya Nagarjuna University, Nagarjuna Nagar- 522 510, India,
[b]RuđerBošković Institute, Division of Materials Chemistry, 10000 Zagreb, Croatia
[c]Faculty of Chemical Engineering and Technology, University of Zagreb, 10000 Zagreb, Croatia
[d]Department of Chemistry, Faculty of Science, University of Zagreb, HR-10000 Zagreb, Croatia
[e]Department of Nanotechnology, Acharya Nagarjuna University, Nagarjuna Nagar- 522 510, India,
[f]Department of Mechanical Engineering, Aditya Institute of Technology and Management, Tekkali 532201, India
[g]Department of Physics, Andhra Loyola College (Autonomous), Vijayawada, A.P., India

Abstract

In this investigations results of dielectric features of Li_2O-Al_2O_3-SiO_2 (LAS) glass doped with 3.0 mol.% of Cr_2O_3, MoO_3 and WO_3 are presented. The investigation spans broad regions of frequency (ω) viz., 10^{-2} -10^{6} Hz and temperature (T) 20-240 °C. Initial characterization of the samples by means of optical absorption spectra revealed that Cr ions do persist in Cr^{3+}oxidation state, whereas fractions of Mo and W ions do present in Mo^{5+} and W^{5+} states besides predominant presence Mo^{6+} and W^{6+} ions, respectively. IR spectra suggested that Mo^{5+} and W^{5+} ions involved in modifying the network of the glass and induced structural disorder. Dielectric parameters and also σ_{ac} were observed to be the largest for LASMo glasses followed by LASW and LASCr glasses. Analysis of dipolar relaxation phenomena were carried out using Cole-Cole plots. Analysis of the results of σ_{ac} suggested polaronic conduction due to electron transfer between $Mo^{5+}\leftrightarrow Mo^{6+}$ and $W^{5+}\leftrightarrow W^{6+}$ is prevailed in case of LASMo and LASW glasses and these glasses are predicted to be useful as cathodes, whereas in LASCr glasses, the ionic conductivity is dominant and are prophesied as suitable for electrolytes in ionic batteries.

***Keywords*:** LAS glass system; $Cr_2O_3/MoO_3/WO_3$ metal oxides; Dielectric features; A.C. conductivity

Corresponding authors: lpavic@irb.hr; vrksurya@rediffmail.com; nvr8@rediffmail.com

1. Introduction

Alumina mixed silicate glasses have a broad range of potential applications owing to their distinctive characteristics, like high thermal and chemical resistances, large mechanical strength etc. These applications include the production of fiberglass, in high-end electronic devices like smartphones for robust and scratch-resistant protective screens, as sealants and as insulators in electrical and industrial equipment. However, the potential uses of these glasses significantly rely on the specific composition of the glass system [1-5].

The introduction of Li_2O in these glass compositions causes rise in their dielectric constant and a reduction in dielectric loss. These characteristics make these glasses suitable for applications at high frequencies and integrated circuits and are also capable of storing electrical energy when subjected to an electric field [6, 7]. In these glasses, SiO_2 participate in the network, through $[SiO_{4/2}]^0$ units with sharing of the 4-oxygens. The modifier oxide viz., Li_2O disrupts Si–O–Si linkages, and causes the development of Si–O terminations. Consequently, the glass structure undergoes depolymerization, resulting different structural units.

Due to its weak glass-forming ability, single-component glass with alumina (Al_2O_3) cannot be readily prepared using conventional melt-quenching techniques. A brief review of recent quantitative studies exploring the fabrication of single-component Al_2O_3 glass by other methods and also the quantitative structural analysis of aluminosilicate glasses. Hashimoto et al. in a novel approach [8] employed electrochemical anodization to create single-component Al_2O_3 glass. Utilizing neutron diffraction and NMR data, they conducted a comprehensive structural analysis of the fabricated glass. Their investigation revealed an avg. Al-O CN as 4.66, along with confirmation of OAl_3 tricluster formation attributable to a significant contribution from common edge of Al-O polyhedrons. This observation challenges the conventional glass network concept proposed by Zachariasen, which relies solely on corner-sharing tetrahedral units, as it demonstrates the existence

of AlO_5 and AlO_6 polyhedrons with common edges. The research by Frankberg et al. revealed surprising ductility in amorphous aluminum oxide (Al_2O_3) at low temperatures. This finding paved the way for the development of damage-resistant glass materials like Al_2O_3 that could significantly improve the mechanical strength and reliability of electronic devices and batteries [9].

Eden and his co-workers have prepared Sc_2O_3–Al_2O_3–SiO_2 system and have performed structural analysis by ^{45}Sc, ^{27}Al, and ^{29}Si NMR studies. Their studies revealed that in addition to AlO_4 tetrahedra, there exists AlO_5 (31%–35%) and AlO_6 (≈5%) polyhedrons in Sc–Al–Si–O glass [10]. Similarly, Stebbins et al. also performed the structural analysis CaO-Al_2O_3-SiO_2 glass with no additional Al over charge-compensating cations. Using ^{27}Al NMR. Their studies revealed the inclusion of ^{5}Al in these glasses and quantified traces of both ^{5}Al and ^{6}Al in in a variety of fluoride-Al_2O_3-SiO_2 glasses [11]. Cormier [12] in his review article on aluminosilicate glasses, reviewed the relationships of composition-structural property by means of NMR technique in a huge number of glasses that include silicate, borate etc along with Al_2O_3. In this article, he identified a variety of structural bondings viz., AlO_4, SiO_4, BO_3 or BO_4units. He further, mentioned that ^{4}Al-O-^{4}Al, ^{4}Al-O-^{4}B and ^{4}B-O-^{4}B interactions are disfavored and they are strongly reliant on and type of cations present in the glass composition.

The studies of nuclear magnetic resonance investigations on alumina-SiO_2 glasses by Rutzet al. revealed that aluminum ions predominantly occupy AlO_4, AlO_6 positions [13] as mentioned below:

$$2Al_2O_3 \rightarrow [Al^{3+}]_o + 3[AlO_{4/2}]_t$$

In general, Al^{3+} in Al_2O_3-SiO_2 network adopts with coordination number (CN) 4 when there are adequate concentration of modifying ions like Li^+ for balancing the charge. The conversion of Al^{3+} from a glass former to modifier with the stoichiometry $(Al^{3+} + Si^{4+})_2O_5^{2-}$ can be written as:

$5Si_2O_5^{2-} + (LiAl)_2O_5^{2-} = 10[(SiO_3)^{2-} / (SiO_{2/2}O_2)^{2-}] + 2\ Li^+ + 2Al^{3+}$

Nevertheless, several earlier investigations on various aluminosilicate glasses mentioned above have indicated that 4-fold coordination is predominates if the content of Al_2O_3 is low, whereas 6-fold coordination is dominant at higher concentrations of Al_2O_3. Regardless of the chosen participation, the CN of Al^{3+} in any glass network causes a swift hike in the intensity of the IR bands associated with Si–O stretchings.

Chromium ions, among the various transition metal ions, exhibit significant effects on the electrical and optical characteristics of glasses. They can be readily integrated into the glass host due to the more flexible and less rigid structure of glass compared to crystalline materials. Irrespective of initial valence state of Cr in the composition, the ions were reported to coexist in various oxidation states within the end product. Glasses containing chromium with mixed oxidation states have recently attracted interest as cathodes in rechargeable batteries due to its remarkable energy concentration and outstanding electrical storage capacity [14-18].

Likewise, the introduction of other transition metal ions of VI B group viz., molybdenum ions, into Li_2O-Al_2O_3-SiO_2 glass increases their chemical as well as corrosion resistance and make them more hard against attack from acids, bases, and other chemicals. Further, physical properties of these glasses are predicted to be substantially influenced by Mo ions and make them highly useful in various optical and electronic devices. Earlier, molybdenum oxide was being used as co-catalyst for the production of acrylonitrile (C_3H_3N) (which is used in plastics, synthetic rubber, acrylic fibres and in pesticides) through the oxidation of C_3H_6 and Al_2O_3. Further, it is considered to be more important oxide because of its layered structure and due to the facile transformation between Mo^{6+} and Mo^{5+} oxidation states. For this reason, its use in electrochemical devices and displays is considered as phenomenal [19, 20].

Furthermore, Mo ions exhibit selective absorption of specific wavelengths of light and significantly influence the optical properties of the host glass. For this reason, the applications of the glasses containing Mo ions are extended in to the manufacturing of tinted glasses and optical filters. Yet, the presence of MoO_3 in the glass materials causes a change in the electrical conductivity to a large extent with respect to pure glass. Based on the quantity of Mo ions and their valence states, these glasses behave as conductors, semiconductors, or insulators and make them useful for a variety of electronic applications [21].

In a similar way, WO_3, an another transition metal oxide of the same group, when doped into Li_2O-Al_2O_3-SiO_2 glasses, changes their optical as well as electrical characteristics to a greater extent. For example, there is an increase of refractive index and makes the glass perfect for optical sensors and other optical devices. Interestingly, glasses with a small quantity of WO_3 exhibit photochromism and electrochromism [22, 23]. Further, the presence of a small quantity of WO_3 influences the magnitude of electrical conductivity and mechanism of conduction of the parent glass largely. In fact, the tungsten ions play an important role in varying the electrical characteristics of glass since the W ions exist in multiple oxidation states viz., 6+, 5+ 4+, in the host glass. Such variations arise due to a reversible thermo-disproportionation equilibrium: $W^{5+} + W^{6+} \leftrightarrow W^{4+} + W^{6+}$, irrespective of its initial valance state [24, 25]. Out of these states, W^{6+} ions become part of network of the glass, forming distinct structural groups such as WO_4 (T_d) and WO_6 (O_h). W^{5+} ($5d^1$) ions combining with O_3^- act as modifiers and, induce disorder in the glass network. Consequently, these glasses exhibit polaronic conduction due to efficient electron transfer between W^{5+} and W^{6+} ions [24, 25] (in addition to ionic component resulted from the transport of Li^+ ions the glass network), This property makes these glasses suitable for applications as electrodes in rechargeable batteries.

The quantitative studies on dielectric characteristics and σ_{ac} of glasses over larger ranges of ω and T provide deep insights into conduction phenomena and structural aspects of amorphous systems. Several quite recent studies explored into such aspects in various glass materials, shed potential information [26-33]. Nevertheless, while there have been large number of studies on structural properties of Li_2O-Al_2O_3-SiO_2 (LAS) glass systems-doped with different *d*-block elemental ions, there exists a significant gap in thorough investigations of dielectric features and σ_{ac} (in wide frequency and temperature regions) of intriguing VIB group oxides (viz., Cr_2O_3, MoO_3, and WO_3) doped lithium aluminosilicate glasses, in the existing literature. Knowledge on such studies is highly useful for the applications of these glasses in the above mentioned devices.

Motivated by these factors, this study focuses on the synthesis of LAS glasses incorporating fixed contents (3 mol.%) of Cr_2O_3, MoO_3, and WO_3 and the evaluation of the structural changes in the glasses due to the addition of these oxides using IR and optical absorption (OA) studies. Finally, we conducted quantitative assessments of a variety of dielectric properties, such as ε, M, and σ_{ac} in a broad ω range (10^{-2} to 10^6 Hz) and in the temperature range 30 – 250 °C. We examined the obtained results in the context of Cr_2O_3, MoO_3, and WO_3 that provide significant insights into the dielectric features of these samples

2. Experimental

The following describes the composition of the studied glasses:

LASCr: $40Li_2O$-$5Al_2O_3$-$52SiO_2$: 3.0 Cr_2O_3

LASMo: $40Li_2O$-$5Al_2O_3$-$52SiO_2$: 3.0 MoO_3

LASW: $40Li_2O$-$5Al_2O_3$-$52SiO_2$: 3.0 WO_3

It is noteworthy that transparent glass containing more than 3.0 mol.% of Cr_2O_3 could not be obtained. The glass samples were synthesized by melt-quenching method. Exact amounts of 99.99% pure compounds of Li_2CO_3, Al_2O_3, SiO_2 (all of Loba Chemie) and the dopants Cr_2O_3,

MoO_3 and WO_3 (obtained from Sigma-Aldrich) were used. The compounds were mixed thoroughly before undergoing melting at 1400 °C for thirty minutes in Pt crucibles within an oxygen-rich environment. After being melted, the molten liquid was poured into brass molds and then annealed at around 350 degree census for roughly six hours to remove imperfections like bubbles and cracks and cooled to ambient temperature over a period of 24 h. During this process the above mentioned defects are predicted to have been eliminated to some extent. Following annealing, the glasses were polished. The glasses of the dimensions 1.0 cm^2 in surface area and t = 0.2 cm are used in this study.

The confirm amorphous state of the prepared samples XRD patterns were recorded and presented Figure 1. No sharp peaks were noticed in these diffractograms and thus revealed the absence of any crystallinity in the samples. SEM images of carbon coated samples were obtained using a Carl Zeiss EvoMA15A microscope. DTA of the samples was conducted on a Mettler TGA/DSC 3+ thermo balance @ a heating 20 °C/min in O_2 atmosphere. EPR spectra were recorded on a JEOL X-band ESR spectrometer (model JES-FA100) with a precision of $7x10^9$ spins/0.6 mT at ambient temperature.

FT-IR spectra were obtained using a Shimadzu IR TRACER 100 spectrophotometer in attenuated reflection (ATR) mode. OA spectra were registered on a JASCO UV-VIS-NIR spectrophotometer, region of 200 – 750 nm. For dielectric measurements (after coating the glasses on both surfaces with thin gold electrodes of a Novocontrol Alpha-AN impudence analyzer was used and such measurements were performed in 0.04 Hz – 1.0 MHz region and in the temperature range 20 to 240 °C with an interval of 5 °C (±0.2 °C). Analysis of impedance plots was performed through equivalent circuit (EC) modeling.

3. Results and Discussion

Table 1 presents data regarding the concentration of Cr^{3+}, Mo^{6+}, and W^{6+} ions, as well as their mean separation in LAS glass system, besides several relevant physical quantities. These parameters were evaluated using density and average molecular weight of the glasses [34].

Since it is usually difficult to observe the presence of nanocrystalline domains within the glass we have recorded HRSEM photographs of titled glasses with the magnification of 500 nm and presented in Figure 2. The photographs indicated entrenchment of crystal grains of nanometer size in the bulk glasses that might have been developed during the melting and annealing of the glasses.

We have also recorded X-ray mappings of the three dopants in these glasses and presented in Figure 3. The mappings demonstrated reasonably homogenous distribution of Cr, Mo and W elements in these glasses. Hence, average transition metal separation presented in Table 1 may be within the acceptable accuracies.

Figure 4 depicts DTA traces of $Cr_2O_3/MoO_3/WO_3$ doped LAS glasses. The thermal traces showed a temperature shift associated with heat absorption, indicating the glass transition occurring between 465 and 475 ^oC. Notably, a distinct release of heat (crystallization peak) is noticeable in range of temperature 610–640 ^oC. The parameter $(T_c\text{-}T_g)$ found to be the largest for LASCr glass (inset of Figure 4) signifying low susceptibility to de-vitrification with respect to LASMo and LASW glasses. In Figure 5a, OA spectra of LASCr, LASMo and LASW glasses were presented. The LASCr glass spectrum indicated absorption edge at 263 nm, whereas for LASMo and LASW glasses the edges were observed, respectively, at 297 and 281 nm. The plots of $(\alpha h\nu)^{1/2}$ vs $h\nu$ Tauc Plots) were drawn to estimate the optical band gap energies (E_o) of the studied glasses (Figure 5b). By extending the linear portions of the plots on to the X-axis, band gaps E_o were estimated for the three glasses. E_o was noticed to be the largest for LASCr (inset of Figure 5b) and the minimum for LASMo glass. The lowest value of E_o obtained for LASMo glass

indicated the higher degree of disorder in the network of this glass while such degree of depolymerization is the minimal in the network of LASCr glass. The smallest value of E_o for LASMo glass is probably due to larger degree of localization of free e^-s, that have enhanced the fraction of donor centres and lead to shrinkage of bandgap.

Additionally, OA spectrum of LASCr glass exhibited a significant band at 625 nm, due to $^4A_2 \rightarrow {}^4T_2$ transition of Cr^{3+} ions. Two faint signatures superposed on $^4A_2 \rightarrow {}^4T_2$ band at 648 and 683 nm, corresponding to the $^4A_2 \rightarrow {}^2T_1$, ^2E (spin and parity forbidden) transitions of Cr^{3+} ions [35] were also detected in this spectrum. However, it may be noted here that chromium ions do exist in 4+, 5+ and 6+ states in addition to 3+ state in amorphous materials as was reported by Kaczmarek [36]. Out of these, the Cr^{6+} ions take part in the glass structure with CrO_4^{2-} units. These Cr^{6+} ions also exhibit an absorption band at about 355 nm, whereas the Cr^{4+} ions are also predicted to exhibit an absorption band in the long wavelength (NIR) region at nearly 1020 nm as we have reported in our earlier papers [37, 38]. Since no such bands are observed in the present spectra (Fig. 5a), the presence of Cr ions in such oxidation states is quite unlikely in this glass.

The presence of a weak peak at 693 nm in the LASMo glass spectrum (see inset for magnified view) suggests Mo^{5+} ion excitation. These ions likely originated from the $Mo^{6+} \rightarrow Mo^{5+} + e^-$ reduction reaction. The formation of molybdenyl complexes from these Mo^{5+} ions is predicted [39] as described by the following chemical equilibrium: $Mo^{6+}+e^- \rightarrow Mo^{5+}$; $_2^- \rightarrow 1/2O_2+2e^-$ (oxygen redox); $Mo^{5+}+O_2^- \rightarrow MoO^{3+}$ (molybdenyl). Mo^{5+} ions are relatively stable and inhabit in octahedral (O_h) sites with Jahn–Teller distortions [40]). These modifying ions create broken bonds in the material and facilitate increased mobility of charge carriers that contribute to σ_{ac}. On the other hand, Mo^{6+} ions involve in the glass network by forming Si-O-Mo and Al-O-Mo bondings [41, 42].

In order to reinforce the observations of optical absorption spectra regarding the valence states of transition metal ions, we have recorded EPR spectra at ambient temperature. The EPR spectrum of LASCr glass (Figure 6(a)) exhibited an intense signal at g = 1.97 originated from pairs of Cr^{3+}–Cr^{3+} centers linked by magnetic dipolar interactions. The spectrum also exhibited another signal at g = 4.7 due to the isolated Cr^{3+} ions. EPR signal on the lower field side (g = 4.7) emerges from isolated Cr^{3+} ions experiencing a distorted octahedral environment [43]. Typically, the signal attributed to the resonance of Cr^{5+} ions was reported at a slightly higher magnetic field compared to that of Cr^{3+} ions. However, this signal can only be detected at liquid nitrogen temperatures [44]. Therefore, it cannot be precisely concluded if chromium ions exist in the Cr^{5+} state based on the current EPR measurements in the examined glasses. Furthermore, the optical absorption spectra also did not indicate the presence of any Cr^{5+} ionic state.

EPR spectrum of MoO_3 doped glass displayed an intense central line along with satellites at $g_{\perp}$ =1.942 and g_{II} =1.889 (Figure 6(b)) predicted due to the resonance of Mo^{5+} ($4d^1$) ions. The central signal arises due to even Mo isotopes (I=0), whereas satellites arising from the hyperfine structure of the odd isotopes viz., ^{95}Mo and ^{97}Mo (I=5/2) [45, 46]. In the optical absorption spectrum of LASMo glass, as discussed earlier, a faint band between 430 and 650 nm, corresponding to the excitation of Mo^{5+} ($4d^1$) ions is noticed. Thus both EPR and OA studies have clearly demonstrated the reduction of partial fraction of Mo^{6+} ions in to Mo^{5+} ions.

In Figure 6c room temperature EPR spectrum of WO_3 doped glasses is presented. The spectrum contained an asymmetrical signal attributed to W^{5+} ions at $g_{\perp}$ =1. 73 and g_{l} = 1. 62. Another weak signal (at larger magnetic field) characteristic of paramagnetic O^- ions was also observed in the low field region [47].

The infrared spectra of these glasses (Figure 7) revealed two primary peaks around 1010 cm^{-1} and 795 cm^{-1}. These peaks correspond to the asymmetric and symmetric stretching vibrations

of Si-O-Si linkages, respectively [42]. In addition, Al-O vibrational band in AlO_6 units at nearly 480 cm^{-1} is also observed; a Si-O-Si rocking vibrational band was also reported in the same region [26]. Band due to AlO_4 vibrational groups is located at nearly780 cm^{-1} [41, 42]. The intensity of this peak is observed to be the highest in the LASCr glass' spectrum. Among the investigated glasses, the LASMo spectrum exhibited the most prominent band corresponding to AlO_6 structural units. Summary of results of IR spectra suggested an increment in the degree de-augmentation among different structural groups when Cr ions were successively replaced by Mo and W ions in LAS glass network.

Real part of dielectric constant (ε') of un-doped LAS glass was measured as152 at 100 ºC and 1 kHz. Upon adding 3 mol.% of Cr_2O_3, this value changed to 180. Under the similar conditions, the value of ε' for the glasses containing 3.0 mol. % MoO_3 was observed to be 286 and for LASW glass it was 213.With decrease of ω up to 0.04 Hz, ε' exhibited significant increase for the three glasses. The variations in ε' with frequency and with temperature for LASCr glass was illustrated in Figures 8a,b, respectively. At temperatures exceeding 100 °C a significant increase in ε' was observed. This increase was highly frequency-dependent, with much larger values observed at low frequency.

The increase of ω resulted in a considerable decrease of ε'. This decrease reached a frequency independent plateau at higher frequencies, represented by $\varepsilon'_\infty(\omega)$, owing to the occurrence of rapid polarization processes within the samples. At such higher frequencies, the conducting species were no longer able to rotate at sufficient speed. As a consequence, their oscillation fell behind the applied field and caused a decrement in $\varepsilon'(\omega)$ and reaches $\varepsilon'_\infty(\omega)$.

With increase of T, $\varepsilon'(\omega)$ indicated a clear dispersal at higher temperatures and showcased higher values at lower frequency. Among different polarizations, space charge polarization (scp) (develops due to filing up of charge carriers at the electrodes), is responsible for the increase of

$\varepsilon'(\omega)$ at low ω. Normally, scp is strongly influenced by the mobility of free charges over long distances which dependence on the degree of structural disorder. In other words, significant raise in $\varepsilon'(\omega)$ at low ω, was a result of relatively free movement ions in the host sample. In contrast, at higher ω, the oscillating frequency of conducting species is comparatively low. This observed discrepancy resulted in ε'(ω) levelling- off at a plateau in the high-frequency regime denoted as $\varepsilon'_{\infty}(\omega)$, as depicted in Figures 8a,b.

Comparison of $\varepsilon'(\omega)$ of the three glasses at any temperature and frequency indicated the minimum value for Cr_2O_3 doped glass and found to be the largest for MoO_3doped glass (Figure 9). Even though, it is possible for Cr ions to be in multiple valence states in the amorphous materials as reported by many authors earlier [17, 18], in the LAS glass matrix it appears to be predominantly in Cr^{3+} state as revealed from OA spectra. These ions like Li^+ ions do act as modifying ions and facilitate rising in the structural de-augmentation of host glass network. Such disorder causes increase of $\varepsilon'(\omega)$ with T especially at lower ω [34].

Glass consisting of 3.0 mol.% of MoO_3, the dielectric parameters, namely ε' and σ_{ac}, exhibited a significant increase at various frequencies and temperatures compared to those of pure glasses and Cr_2O_3 doped glasses. As mentioned earlier, the optical absorption spectra indicated a fraction of Mo ions do exist in pentavalent state. Such Mo^{5+} ions function as modifiers, create broken bonds in the glass and pave the way for easy trajectories for the diffusion of charges, leading to the build-up of scp and causes to enhance the value of ε' [48, 49].

W ions typically persist in the W^{6+} state, involve in the glass with tetrahedral (WO_4) and octahedral (WO_6) units [50-52]. Moreover, there is an evidence from optical absorption and EPR spectral results for the presence of a fraction of these ions in W^{5+} state within the glass matrix,. It is anticipated that W^{5+} ions predominantly occupy interstitial positions due to the substantial ratio of cation-oxygen radii, which is 0.45 for W^{5+} ions. This ratio significantly differs from 0.19 required

for any ion to occupy tetrahedral sites [50-52]. Like Li^+ ions, W^{5+} ions also behave as modifying ions. The WO_4 groups linked to SiO_4 groups, form Si-O-W linkages. The introduction of Li^+ modifying ions causes breaking of such linkages, leading to a reaction represented as Si-O-W + $Li_2O \rightarrow$ Si-O-Li^+ + WO-Li^+. Additionally, the W^{5+} ions, act as modifiers, disrupt the mentioned bonds by creating bonding defects that contribute to scp and cause to increase ε'. However, the magnitude of this polarization appears to be relatively lower compared to that observed in glasses doped with MoO_3. The variations of imaginary part of $\varepsilon''(\omega)$ for the three glasses either with frequency or with temperature exhibited a similar behavior.

To gain a clear picture of the inherent dipolar effects of these glasses, we have used the notation of electrical modulus. This approach offers a notable advantage: it minimizes the impact of electrode polarization effects within the system, as outlined in Refs. [53-57].

Accordingly, the complex electric modulus is denoted as:

$$M^*(\omega) = \frac{1}{\varepsilon^*(\omega)} = M_\infty \left[1 - \int_0^\infty \frac{-d\varphi(t)}{dt} exp(-i\omega t)\, dt\right]$$

$$= M'(\omega) + i\, M''(\omega) \qquad (1)$$

By separating real and imaginary components, we get

$$M'(\omega) = M_\infty M_s \frac{\left[M_s A^\beta + (M_\infty - M_s)\cos\beta\varphi\right]A^\beta}{M_s^2 A^{2\beta} + 2A^\beta (M_\infty - M_s)M_s \cos\beta\varphi + (M_\infty - M_s)^2}$$

$$= \frac{\varepsilon'(\omega)}{(\varepsilon'(\omega))^2 + (\varepsilon''(\omega))^2} \qquad (2)$$

$$M''(\omega) = M_\infty M_s \frac{[(M_\infty - M_s)\, sin\,\beta\varphi]A^\beta}{M_s^2 A^{2\beta} + 2A^\beta (M_\infty - M_s)M_s\, cos\,\beta\varphi + (M_\infty - M_s)^2}$$

$$= \frac{\varepsilon''(\omega)}{(\varepsilon'(\omega))^2 + (\varepsilon''(\omega))^2}\ . \qquad (3)$$

where $M_s = 1/\varepsilon_s$, $M_\infty = 1/\varepsilon_\infty$ and

$$A = \left[1 + 2(\omega\tau_0)^{1-\alpha} \sin\left(\frac{\alpha\pi}{2}\right) + (\omega\tau_0)^{2(1-\alpha)}\right]^{1/2} \qquad (4)$$

$M'(\omega)$ and $M''(\omega)$ components were computed by substiting the measured values of $\varepsilon'(\omega)$ and $\varepsilon''(\omega)$ in the equations (3) and (4).

Figure 10 displays the plots of $M'(\omega)$ and $M''(\omega)$ *vs* ω and Figure 11 represent their variations with T for the titled glasses. These figures vividly revealed the dielectric relaxation character of these glasses. Notably, $M'(\omega)$ demonstrated an increase with rising temperature and eventually levels off at sufficiently high temperatures, indicating the attainment of the limiting value denoted as M_∞. Additionally, the peak in $M''(\omega)$ shifts to higher ω with the raise temperature. The frequency range below the maximum of $M''(\omega)_{max}$ signifies the movement of conducting species for larger distances. When frequencies exceeding $M''(\omega)_{max}$, ions become trapped within potential wells. This restricts their movement, causing them to oscillate locally within these wells and significantly reducing their ability to transport for longer distances.

The frequency corresponding to the intersection of $M''(\omega)$ and $M'(\omega)$ is denoted as ω_{max} and the relaxation time, τ_M of dipoles is evaluated using $\omega_{max} = 1/\tau_M$ (Figure 12). Significantly, LASMo glass displayed considerably lower τ_M values at any specific temperature, whereas LASCr glass exhibited the highest value of τ_M. Table 2 provides detailed information on the relaxation times along with other pertinent of the glasses clearly showcasing these distinct differences.

In insulating materials, the relaxation phenomena is associated with dipolar polarization which strongly dependent on ω in the low ω range. The orientation of inherent dipoles towards electric field plays a significant role in such polarization. Nevertheless, with increase of ω, there is a hindrance for the alignment of dipoles. Such hindrance diminishes their contribution to orientation polarization and causes decrease of $\varepsilon'(\omega)$ with increase of ω . In glasses exhibiting

polaronic conductivity, electrons are engaged in strong interactions with glass-network, giving rise to small polarons. These polarons create localized regions of +ve and -ve charge, acting like tiny dipoles in the bulk glass. Particularly, the electron involved in forming a polaron is also the one which can hop between sites, allowing the conduction in the glass at lower frequencies, which will be discussed in depth at the later stage in this manuscript. Upon encountering the potential well, the polaron undergoes effective confinement, resulting in orientation polarization. M' and M'' components were standardized relative to M'_{∞} and M''_{max}, respectively, and were plotted against log (ω/ω_{max}) in the region of 20-60 °C for LAS: Cr_2O_3/MoO_3/WO_3 glasses in Figure 13. The obtained spectra confirmed a non-dispersal master curve. However, attempts to replicate such master curves at elevated temperatures proved unachievable. These curves suggest a negligible impact of T (up to 60 °C) on relaxation character.

To gain deeper insights into dipolar phenomena, Cole-Cole plots viz., M' vs M'' were drawn in the temperature range 30-100 °C (Figure14) for the titled glasses. The obtained diagrams appeared to be semi-circular shapes with centers depressed beneath the X-axis. However, the plots drawn above 100 ^{o}C were observed to deviate from the semi-circles. Angle (α') subtended by the line connecting the arc's center to the origin on the X-axis was measured and presented in Table 2. α' was identified to be the lowest for LASCr samples and the maximal LASMo glass indicating the distribution of relaxation time (τ) as narrower for the LASCr glass compared to that of LASMo glass. This observation suggests a more rigid environment for the dipoles in LASCr glass. This view point was also supported by the results of IR studies. Such broadening of relaxation times indicates the glasses consist of dipoles with different magnitudes of dipole moments. Furthermore, even those with same magnitude of dipole moments, if entrenched in different potential regions, also contribute significantly to such spreading. Additionally, in LASMo and LASW glass samples $(Mo^{5+}O_3)^-$ and $(W^{5+}O_3)^-$ complexes which were reported to have net-dipole moment and contribute to

relaxation behaviour [58, 59]. These factors combined offer an explanation for the observed spread in relaxation time. Such spreading factor is observed to be the largest for MoO_3 doped glasses indicating more degree of de-augmentation of various structural units in this glass network or more disorder that facilitate more freedom for the dipoles to oscillate.

In Figures 15 and 16 plots of Z' (real) and Z'' (imaginary) components of impedance respectively, against ω presented for all three glasses. Among these components, Z' displayed a decreasing tendency with frequency, with a slight disproportionality in the low frequency region due to electrode effect. However, Z'' showed substantial dispersion with T in the lower ω region (< 1 kHz). In mid frequency region, Z'' demonstrated a linear raise with frequency. Nearly about 100 kHz, Z'' is found to vary inversely with ω.

To comprehend the influence of $Cr_2O_3/MoO_3/WO_3$ on the magnitude of Z in these glasses, Nyquist plots, viz., Z'' vs Z', were drawn in 20-60 ^oC region of temperature and illustrated in Figure17 for the three studied glasses. It may be note that beyond 60 ^oC closed semi-circular arcs could not be obtained. The comparison plot of Z'' against Z' drawn at 20 ^oC (presented in the same figure) indicated the minimal area under the curve for LASMo glasses, suggesting the minimum impedance of this glass among the three glasses. The graphs exhibited a characteristic signature: semi-circular arcs with an inclined spur, especially at low frequencies and higher temperatures. This behavior may be ascribed to the thermally stimulated motion of conducting species at higher temperatures.

To further elaborate the impedance behavior, Bode plots, representing ($|Z|$) and phase angle (ϕ = arc tan ($-Z''/Z'$)) vs ω, were constructed and are depicted in Figure 18 for the glass LASMo at 100 °C. The plot indicated lowering of $|Z|$ as ω is increased, suggesting that the electronic (or Faradic) current made a significant addition to the impedance [60, 61]. The phase angle ϕ was found to vary from -5 to -73 degrees as the frequency is increased up to 1 MHz. This change in ϕ signifies a

gradual shift in the impedance of the material from behaving more like a resistor (R) to acting more like a capacitor. The observed reduction in capacitive effects at lower frequencies likely originates from a combination of factors. These factors could include interfacial polarization, on-ideal contact characteristics between electrodes, or the presence of electrode polarization resistance.

Figures 19a, b, respectively, depict the variations of σ_{ac} with frequency and inverse temperature (*1/T*) for these samples. At a low ω region, σ_{ac} demonstrated a linearity with *1/T*, becoming nearly invariant with *T* at higher frequency and low temperatures. A comparison of σ_{ac} at 200 °C and 1000 Hz (Figure 20) revealed the highest conductivity for MoO_3-doped glass among the investigated glasses. Using the plots log σ_{ac} *vs 1/T*, the activation energy (W_{ac}) for conduction was evaluated at 1kHz and 400 K. W_{ac} was found to be lowest for LASMo glass, while it was found to be the largest for Cr_2O_3-mixed glass (Table 2). This observation suggests a larger degree of internal chaos in the network of LASMo glass that facilitated higher conductivity.

At low frequencies and high temperatures, σ_{ac} demonstrated near frequency-invariance. Nevertheless, at large frequencies, σ_{ac} is found to obey the relation, $\sigma_{ac} \propto \omega$. In the middle ω region, σ_{ac} is observed to follow *viz*., $\sigma_{ac} \propto \omega^s$ relation, where $s < 1$, known as UDR (universal dielectric response) exponent. Figure 21 depicts plots log σ_{ac} vs log ω drawn at different temperatures in the range of 20 - 140 °C for the studied glasses. The exponent value, evaluated using the tangent value of such graphs, exhibited a decrease with increase of *T* (Figure 21 inset drawn for the glass LASMo), suggesting that the polarons' tunneling is predominant contribution to σ_{ac}. Such plots of the other two samples revealed the maximal *s* value for LASCr glass and minimal for LASMo glass (Table 2), suggesting that the accessible free space for conducting species to transport is the largest in LASMo glass [62, 63].

In the mid-frequency range, the conducting species undergo oscillatory hopping due to Coulombic repulsion. OA and EPR spectra revealed that Mo ions do exist Mo^{5+} and Mo^{6+} valance states and W ions in W^{5+} and W^{6+} valance states in LASMo and LASW glasses, respectively. This implies that possible polaronic exchange between $Mo^{5+} \leftrightarrow Mo^{6+}$ and $W^{5+} \leftrightarrow W^{6+}$ ions contributing to σ_{ac}. These findings suggest that LASCr glass primarily exhibits ionic conductivity, making it suitable as an electrolyte. Conversely, when MoO_3 replaces Cr_2O_3, polaronic conduction due to SPH is predominant, making the LASMo is more suitable for electrodes in solid state batteries.

In amorphous materials electrical conduction can occur through several mechanisms. These include movement of charges within continuous energy bands (band conduction), transport through extended states, and hopping of charges between localized states near the band edges and the Fermi level (E_F). Among these, the localized states near the E_F are of particular significance, playing a crucial role in the temperature independent region of σ_{ac} irrespective of temperature (in the low-temperature range) and displayed a linear correlation with ω. This precise mechanism of conduction may be ascribed to the examined Li_2O-Al_2O_3-SiO_2:Cr_2O_3/MoO_3/WO_3 glass system, particularly up to 365 K, and at ω greater than 100 Hz (see Figure 19).

It has been previously mentioned that the electrical conductivity (σ_{ac}) with temperature in the lower temperature region, especially at larger frequency range, remains nearly constant. In this region this range, we have analyzed the characteristics of σ_{ac} using the quantum mechanical tunneling (QMT) model [64]. This model allowed to determine the density of defect energy states ($N(E_F)$) near the Fermi energy (E_F) using,

$$\sigma(\omega) = \frac{\pi}{3} e^2 k_B T [N(E_F)]^2 \alpha''^{-5} \omega \left[ln \frac{\nu_{ph}}{\omega} \right]^4 \qquad (5)$$

In Equation (5), $\left[\ln\left(\frac{\nu_{ph}}{\omega} \right) \right]$ represents the hopping range of the charge carriers. The specifications of other symbols in Equation (5) were reported in Ref. [62]. The values of $N(E_F)$

were determined with Equation (5) at 105 kHz and at 355 K, with $\alpha'' \approx 0.65$ Å^{-1} (evaluated using log σ_{ac} versus R_i plots), and furnished in Table 2. The minimum $N(E_F)$ value observed for LASCr glasses indicates relatively smaller fraction of induced defects in this glass network, whereas it is found to be the maximal for LASMo glass. This outcome is consistent with the findings of spectroscopic studies.

4. Conclusions

LAS glasses viz., Li_2O-Al_2O_3-SiO_2 doped with 3.0 mol.% of VIB group elemental oxides (Cr_2O_3, MoO_3 and WO_3) were synthesized. The optical absorption spectra revealed that Cr ions do exist in trivalent state, whereas a fraction of Mo and W ions do exist in Mo^{5+} and W^{5+} valance states besides Mo^{6+} and W^{6+} states. IR spectral investigations suggested that aluminum ions occupy tetrahedral and octahedral positions. These studies further indicated larger degree of disorder in the glass networks of LASMo and LASW attributed to modifying action of $(Mo^{5+}O_3)^-$ and $(W^{5+}O_3)^-$ complexes. Different dielectric and conductivity parameters measured in broad ranges of frequency and temperature suggested the highest values for LASMo glass among the three glasses studied and the lowest values for LASCr glass. However, the impedance exhibited an opposite trend for these glasses. Quantitative analysis of dipolar effects established through the plots of electric moduli and Cole-Cole diagrams, indicated the minimal value of dipole relaxation time (τ) for LASMo glasses. The dipolar phenomena were attributed to the $(Mo^{5+}O_3)^-$ and $(W^{5+}O_3)^-$ complexes with oxygen ions in addition to entrenchment of dipoles in the regions of varied magnitudes of potential in host glass. The results of conductivity studies suggested larger magnitude of ionic contribution to the conductivity in case of LASCr glass, whereas polaronic conduction appeared to be prevalent in LASMo and LASW glasses attributed to the electron transfer from Mo^{5+} to Mo^{6+} and W^{5+} to W^{6+}states. From these observations it is concluded that

LASCr glass is more suitable as electrolytes, whereas LASMo and LASW glasses were predicted as useful for electrodes in ionic batteries.

References

1. J. Wu, Y. Li, Y. Zhao, Z. Li, A. Lu, J. Non-Cryst. Solids **2022**, 583, 121469.

2. A. Ananthanarayanan, G.P. Kothiyal, L. Montagne, B. Revel, J. Solid State Chem. **2010**, 183**,** 120.

3. A. Hamdan, A. Hajimohammadi, B. Njegic, T. Kim, Cem. Concr. Res. **2023***,* **166**, 107103.

4. Y. Gandhi, M.V. R. Rao, C.S. Rao, I.V. Kityk, N. Veeraiah, J. Lumin. **2011**, 131, 1443.

5. C.S. Rao, V. Ravi Kumar, T. Srikumar, Y. Gandhi, N. Veeraiah, J. Non-Cryst. Solids **2011,** 357, 3094.

6. R. P. Ramasamy, P. Ramadass, B. S. Haran, B.N. Popov, J. Power Sources **2007**, 166, 266.

7. M.S. Shalaby, Mohammed O. Alziyadi, H. Gamal, J. Alloys Compd. **2023**, 969, 172318.

8. H. Hashimoto, Y. Onodera, S. Tahara, S. Kohara, K. Yazawa, H. Segawa, M. Murakami, K. Ohara, Sci. Rep. **2022**, 12, 516.

9. E.J. Frankberg, J. Kalikka, F. GarcíaFerré, L. Joly-Pottuz, T. Salminen, J. Hintikka, M. Hokka, S. Koneti, T. Douillard, B. Le Saint, P. Kreiml, M.J. Cordill, T. Epicier, D. Stauffer, M. Vanazzi, L. Roiban, J. Akola, F. Di Fonzo, E. Levänen, K. Masenelli-Varlot, Science **2019**,366, 864.

10. B. Pahari, S. Iftekhar, A. Jaworski, K. Okhotnikov, K. Jansson, B. Stevensson, J. Grins, M. Edén, J. Am. Ceram. Soc.**2012,** 95, 2545.

11. J.F. Stebbins, S. Kroeker, S.K. Lee, T.J. Kiczenski, J. Non-Cryst. Solids **2000**, 275 1.

12. L. Cormier, Glasses: Aluminosilicates. Encyclopedia of Materials: Technical Ceramics and Glasses, Elsevier, **2021.**

13. H.L. Rutz, D.E. Day, C. F. Spencer, J. Am. Ceram. Soc. **1990,** 73, 1788.

14. B.M. Casari, E. Wingstrand, V. Langer, J. Solid State Chem. **2006,** 179, 296.

15. D. Liu, X. Mu, R. Guo, J. Xie, G. Yin, P. Zuo, Int. J. Electrochem. Sci. **2023**, 18, 44.

16. C.M. Harrison, P.R. Slater, R. Steinberger-Wilckens, Solid State Ionics **2020,** 20, 115410.

17. H.Y. Morshidym, A. R. Mohamed, A.A. Abul-Magd, M.A. Hassan, Mater. Chem. Phys.**2022,** 285, 126128.

18. B.V. Raghavaiah, N. Veeraiah, Phys. Status Solidi A**2023**, 199, 389.

19. A.V. Ravi Kumar, C.S. Rao, G. Murali Krishna, V. Ravi Kumar, N. Veeraiah, J. Mol. Struct. **2012**, 1016, 39.

20. F. F. Ferreira, T. G. S. Cruz, M. C. A. Fantini, M. H. Tabacniks, S. C. de Castro, J. Morais, A. de Siervo, R.Landers, A. Gorenstein, Solid State Ionics **2000***,* 357, 136.

21. R. U. Singh, K. Chandra Sekharm, J. S. Alzahrani, Z.A. Alrowaili, Md. Shareefuddin, Y. Purushotham, I.O. Olarinoye, I.O. Olarinoye, M.S. Al-Buriahi, Ceram. Int.**2023,** 49, 11600.

22. L.U. Krüger, C.M. Cholant, J.A. Gomez, D.M. Landarin, C.S. Lucio, D.F. Lopes, L.O.S. Bulhões, C.O. Avellaneda, Opt. Mater. **2022,** 128, 112357.

23. O. Ejeromedoghene, O. Oderinde, S. Adewuyi, G. Fu, React. Funct.Polym.**2023,** 186, 105553.

24. P. Suttiyarak, S. Buathet, A. Tubtimtae, Optik **2020**, 212, 164662.

25. K. Sambasiva Rao, M. Srinivasa Reddy, V. Ravi Kumar, N. Veeraiah, Mater. Chem. Phys. **2008**, 18, 283.

26. T.V.N. KeertiKut, A. Bafti, J. Pisk, L. Pavi´c, A. VenkataSekhar, P. Naresh, A. Siva Sesha Reddy, G. Naga Raju, V. Ravi Kumar, N. Veeraiah, J. Non-Cryst. Solids **2023**, 599,121954.

27. S. Alsowidy,Ahmed M. Aljarbani,Mohammed S. Gumaan, Results Mater. **2022,** 16,100319.

28. F.A. Abdel-Wahab, M. Abdel-Baki, J. Non-Cryst. Solids **2009**, 355, 2239.

29. L Pavić, N. N. Rao, A. Moguš-Milanković, A. Šantić, V. Ravi Kumar, M. Piasecki, I.V. Kityk, N. Veeraiah, Ceram. Int. **2014,** 40, 5989.

30. K. Sambasiva Rao, M. Srinivasa Reddy, V. Ravi Kumar, N. Veeraiah, Physica B **2007,** 396, 29.

31. A. Siva Sesha Reddy, M.G. Brik, J. Suresh Kumar, M.P.F. Graça, G. Naga Raju, V. Ravi Kumar, M. Piasecki, N. Veeraiah, Ceram. Int. **2016**, 42, 17269.

32. S. Vijaya Krishna, L. Pavić, A. Bafti, J. Pisk, D Bhadrarao, Y Dana Rao, A Venkata Sekhar, V Ravi Kumar, N Veeraiah, Appl. Phys. **2024,** A, 130), 1-16

33. V. Prasad, Luka Pavić, Andrea Moguš-Milanković, A. Siva Sesha Reddy, Y. Gandhi, V. Ravi Kumar, G. Naga Raju, N. Veeraiah, J. Alloys Compd. **2019**, 773, 654-665

34. M. M. Ahmed, C. A. Hogarth, M. N. Khan, J. Mater. Sci. **1984,** 19, 4040.

35. M. Rami Reddy, V. Ravi Kumar, N. Veeraiah, Ind. J. Pure & Appl. Phys. **1995**, 33, 48.

36. S.M. Kaczmarek, $Li_2B_4O_7$ glasses doped with Cr, Co, Eu and Dy, Opt. Mater. **2002**, 19, 189.

37. M. Srinivasa Reddy, S. V. G. V. A. Prasad, and N. Veeraiah, Phys. Stat. Sol. A **2007**, 204, 816.

38. G. Murali Krishna, B. AnilaKumari, M. Srinivasa Reddy, N. Veeraiah, J. Solid State Chem. **2007**, 180, 2747.

39. P. Syam Prasad, M. Srinivasa Reddy, V. Ravi Kumar, N. Veeraiah, Philos. Mag. **2007,** 87, 5763.

40. V.V. Sliznev, O.A. Pimenov, G.V. Girichev, J. Mol. Struct. **2020,** 1199, 126884.

41. K.J. Rao, Structural Chemistry of Glasses, Elsevier, Amsterdam **2002**.

42. Y. Gandhi, M.V. Ramachandra Rao, Ch. Srinivasa Rao, I.V. Kityk, N. Veeraiah, J. Lumin. **2011,** 131, 1443.

43. E.V. Zamyatinaa, V.V. Karzanova, O.A. Zamyatina, J. Non-Cryst. Solids **2000**, 528, 119759.

44. M. Srinivasa Reddy, S.V.G.V.A. Prasad, N. Veeraiah, Phys. Stat. Solidi A **2007**, 204, 816.

45. O. Cozar, I. Ardelean, S. Simon, L. David, Solid State Commun. **1993,** 85, 461.

46. P. Syam Prasad, B.V. Raghavaiah, R. Balaji Rao, N. Veeraiah Solid State Commun. **2004,** 132, 235.

47. P. Subbalakshmi, B.V. Raghavaiah, R. Balaji Rao, N. Veeraiah, EPJ Appl. Phys.**2004**, 26, 169.

48. B. Vijaya Kumar, T. Sankarappa, Santosh Kumar, M. Prashant Kumar, P.J. Sadashivaiah, R. Ramakrishna Reddy, Physica B **2009,** 404, 3487.

49. G. Srinivasarao, N. Veeraiah, J. Solid State Chem. **2002,** 166, 104.

50. A.A. Bhagat, M.M. El-Samanoudy, J. Phys. Chem. Solids **1999**, 60, 1921.

51. G. Poirier, M. Poulain, Y. Messaddeq, S.J.L. Ribeiro, J. Non-Cryst. Solids **2005,** 351, 293.

52. P. Subbalakshmi, N.Veeraiah, J. Non-Cryst. Solids **2002,** 298, 89.

53. M. Nagarjuna, T. Satyanarayana, V. Ravi Kumar, N. Veeraiah, Physica B **2009,** 404, 3748.

54. N.G. Mc. Crum, B.E. Read, G. Williams, An elastic and dielectric effects in polymeric solids Wiley, London 1967.

55. G.M. Tsangaris, G.C. Psarras, N. Kouloumbi, J. Mater. Sci. **1998,** 33, 2027.

56. S.J ani Basha, M. Kostrzewa, A. Ingram, A. Siva Sesha Reddy, N. Purnachand, V. Ravi Kumar, M. Piasecki, N. Veeraiah. J. Non-Crystal. Solids **2019**, 521, 119529

57. V. Prasad, M. Kostrzewa, Y. Gandhi, A. Ingram, B. Suresh, A. Siva Sesha Reddy, V Ravi Kumar, N. Veeraiah, Physica B, **2019**, 566, 136-145

58. G.C. Psarras, E. Manolakaki, G.M. Tsangaris, Compos Part A: Appl. Sci. Manuf. **2002,** 33, 375.

59. P. Naresh, G. Naga Raju, M. Srinivas Reddy, T. Venkatappa Rao, I.V. Kityk and N. Veeraiah, J. Mater. Sci.: Mater. Electron. **2014**, 25, 4902-4915.

60. Y. Gandhi, K.S.V. Sudhakar, M. Nagarjuna and N. Veeraiah, J. Alloys. Compd. **2009**, 485, 876-886

61. F. Fasmin, R. Srinivasan, J. Electrochem. Soc. **2017,** 164, H443.

62. J. Ashok, N. Purnachand, J. Suresh Kumar, M. Srinivasa Reddy, B. Suresh, M.P.F. Graça, N. Veeraiah, J. Alloys Compd. **2017,** 696, 1260.

63. C. Filipič, A. Moguš-Milanković, L. Pavić, K. Srilatha, N. Veeraiah, A. Levstik, J. Appl. Phys. **2012,** 112, 073705.

64. G. Austin and N.F. Mott, Adv. Phys. **2001,** 50, 757.

Caption for Tables

Table 1. Physical parameters of Cr_2O_3, MoO_3 and WO_3 doped Li_2O-AL_2O_3-SiO_2 glasses.

Table 2. Summary of the data on a.c. conductivity and other related parameters of Cr_2O_3, MoO_3 and WO_3 doped Li_2O-Al_2O_3-SiO_2 glasses.

Caption for figures

Figure 1. XRD patterns of Li_2O-Al_2O_3-SiO_2:Cr_2O_3/MoO_3/WO_3glasses recordedin the 2 theta range 15‑65 degrees with a scanning rate of 0.02 deg/s.

Figure 2.SEM photographs of Li_2O-Al_2O_3-SiO_2 glasses doped with (a) Cr_2O_3, (b) MoO_3 and (c)WO_3 glasses recorded with a magnification of 500 nm.

Figure 3. X-ray mappings of Cr, Mo, W elements in Li_2O-Al_2O_3-SiO_2 glasses.

Figure 4. Traces of differential thermal analysis (DTA) of Li_2O-Al_2O_3-SiO_2:Cr_2O_3/MoO_3/WO_3 glasses, revealing glass transition (T_g) and and crystallization temperatures. (Tc). Inset represents the values of (Tc–Tg) for the three glasses.

Figure 5a. Optical absorption spectra of Li_2O-Al_2O_3-SiO_2:Cr_2O_3/MoO_3/WO_3glasses recorded at ambient temperature with the indication of electronic transitions dopant ions. The insets highlight magnified views of peaks specific to LASMo and LASW glasses.

Figure 5b. The plots of $(\alpha h\nu)^{1/2}$ versus $h\nu$ (Tauc Plots) drawn to estimate the optical band gap energies (E_o) of Li_2O-Al_2O_3-SiO_2: Cr_2O_3/MoO_3/WO_3 glasses. The inset compares E_o values for all three studied glasses.

Figure 6. EPR spectra of Li_2O-Al_2O_3-SiO_2 glasses doped with **a** Cr_2O_3, **b** MoO_3 and **c** WO_3 recorded at ambient temperature.

Figure 7. Fourier Transform Infrared (FT-IR) spectra of Li_2O-Al_2O_3-SiO_2:Cr_2O_3/MoO_3/WO_3 glasses recorded in attenuated total reflection (ATR) mode, providing information on vibrational bands of specific functional groups.

Figure 8. Variations of dielectric constant (ε') of LASCr glasses (a) with frequency measured at different temperatures and (b) with temperature measured at different frequencies illustrating the material's response to frequency of the applied electric field and temperature dependence of the material's dielectric properties.

Figure 9. Comparison of dielectric constant at 100 °C and 1 kHz for Li_2O-Al_2O_3-SiO_2 glasses doped with 3.0 mol.% of Cr_2O_3, MoO_3, and WO_3, highlighting the influence of dopant type on dielectric behaviour.

Figure10. Variations of real (M') and imaginary (M") parts of electric moduli with frequency for LASCr, LASMo, and LASW glasses measured at different temperatures.

Figure11. Variations of real and imaginary parts of electric moduli with temperature for Li_2O-Al_2O_3-SiO_2 glass doped with 3.0 mol.% of Cr_2O_3, MoO_3, and WO_3, revealing the combined effect of temperature and dopant on the material's response.

Figure 12. Plots of real and imaginary parts of electric moduli with frequency at 100 °C for LASCr, LASMo, and LASW glasses, used to estimate the relaxation time of each material.

Figure 13. Scaling behavior of electric moduli with temperature for Li_2O-Al_2O_3-SiO_2: Cr_2O_3/MoO_3/WO_3 glasses between 20°C and 60°C, demonstrating the consistency of the response across different temperatures.

Figure 14. Cole-Cole plots for Li_2O-Al_2O_3-SiO_2 glass doped with Cr_2O_3, MoO_3, and WO_3 measured between 30°C and 100°C, visualizing the relaxation processes .

Figure 15. Variations of real part (Z') of electrical impedance with frequency for Li_2O-Al_2O_3-SiO_2: Cr_2O_3/MoO_3/WO_3 glasses measured at different temperatures, indicating the resistive behavior of the materials.

Figure16. Variations of imaginary part (Z") of electrical impedance with frequency for Li_2O-Al_2O_3-SiO_2: Cr_2O_3/MoO_3/WO_3 glasses measured at different temperatures, depicting the reactive behavior of the materials.

Figure 17. Plots of Z" vs Z' for LASCr, LASMo, and LASW glasses drawn in the temperature regions 20-60 °C, along with equivalent circuit model, representing the distribution of resistive and capacitive components within the materials.

Figure18. Bode plots of total impedance (|Z|) and phase angle (φ) for LASMo glass drawn at 100°C, providing a comprehensive view of the frequency-dependent electrical response.

Figure 19a. Variation of log σ_{ac} with frequency (measured at different temperatures) of Li_2O-Al_2O_3-SiO_2 glasses doped with Cr_2O_3, WO_3 and MoO_3.

Figure 19b. Variation of σ_{ac} with inverse temperature (1/T) for Li_2O-Al_2O_3-SiO_2: Cr_2O_3/MoO_3/WO_3 glasses, drawn for evaluation of the activation energy required for charge conduction.

Figure 20. Comparison of σ_{ac} at 200°C and 1 kHz for Li_2O-Al_2O_3-SiO_2 glasses doped with 3.0 mol.% of Cr_2O_3, WO_3, and MoO_3, highlighting the impact of dopant on conductivity.

Figure 21. Variation of log σ_{ac} with log ω for Li_2O-Al_2O_3-SiO_2: Cr_2O_3/MoO_3/WO_3 glasses, used to determine the exponent *s* in the power law relationship, indicating the conduction mechanism at different temperatures. The inset shows the temperature dependence of *s* for LASMo glass..

Table 1. Physical parameters of Cr_2O_3, MoO_3 and WO_3 doped Li_2O-Al_2O_3-SiO_2 glasses.

Glass Sample	Density (g/cm^3)	Conc. $Cr^{3+}/Mo^{6+}/W^{6+}$ ions Ni ($\times 10^{20}/cm^3$)	Inter ionic distance Ri (Å)
LASCr	2.83	9.67	10.11
LASMo	2.75	9.45	10.18
LASW	2.79	9.12	10.30

Table 2. Summary of the data on a.c. conductivity and other parameters of Cr_2O_3, MoO_3 and WO_3 doped Li_2O-Al_2O_3-SiO_2 glasses.

Glass	Exponent *s* *at* 100 ºC	$N(E_F)$ ($\times 10^{21}$,eV^{-1}/cm^3)	A.E. for conduction, W_{ac}(eV) at 1kHz, 373K	Relaxation time, τ_M(μs)	A.E. for dipoles, W_d(eV)	Spreading factor α' (rads)
LASCr	0.18	3.07	0.49	2.05	1.81	0.129
$LASM_o$	0.13	4.81	0.38	1.24	1.75	0.017
LASW	0.15	4.55	0.40	1.31	1.79	0.096

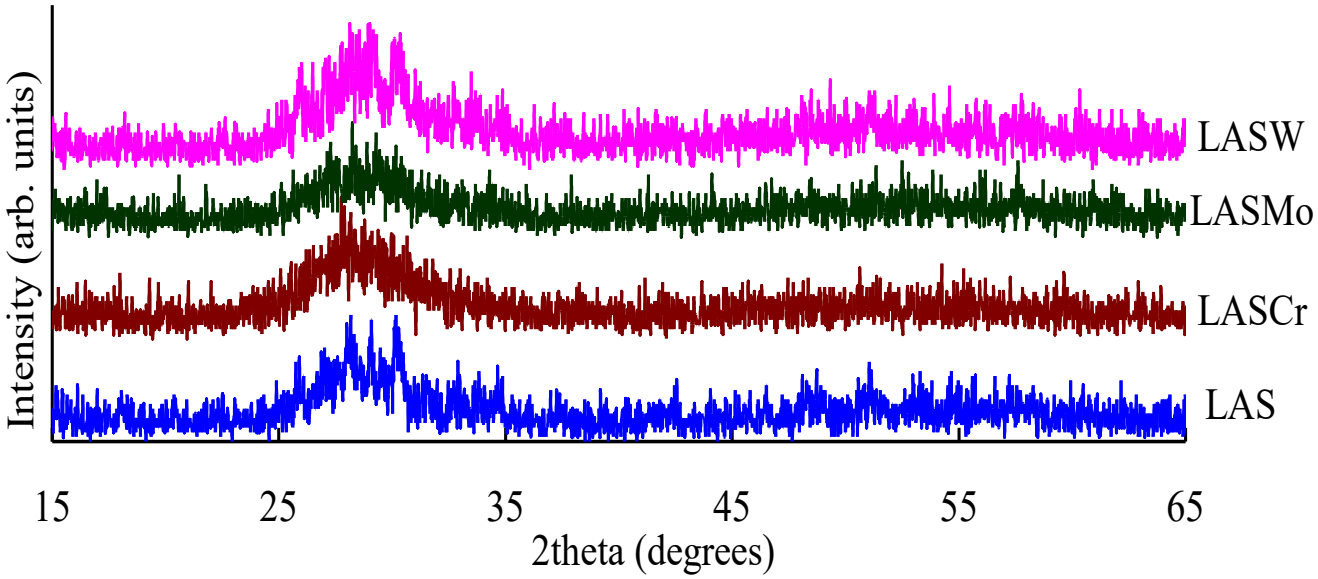

Figure 1. XRD patterns of Li_2O-Al_2O_3-SiO_2:Cr_2O_3/MoO_3/WO_3glasses recorded in the 2 theta range 15‑65 degrees with a scanning rate of 0.02 deg/s.

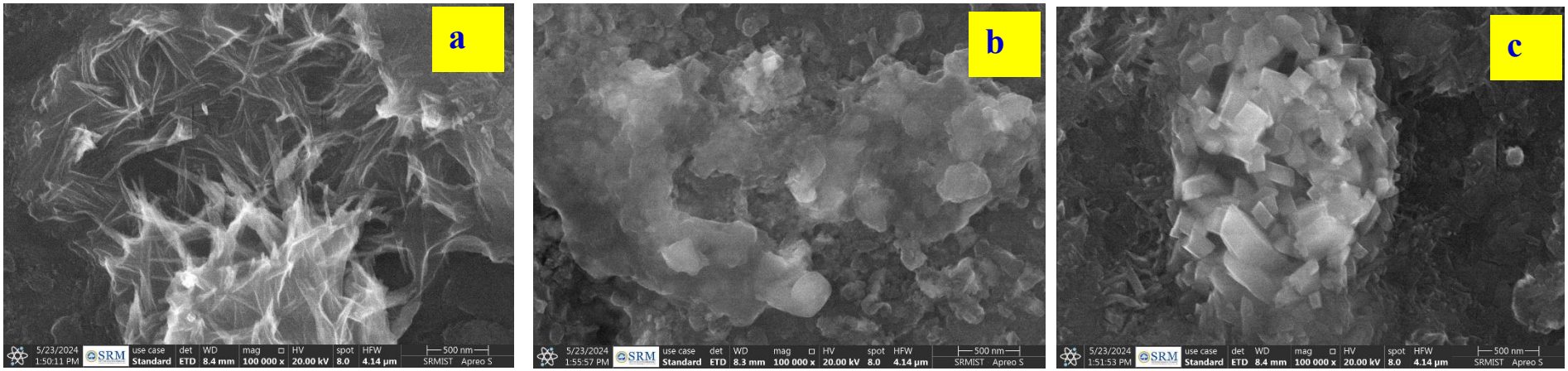

Figure 2b. SEM photographs of Li_2O-Al_2O_3-SiO_2 glasses doped with (a) Cr_2O_3, (b) MoO_3 and (c)WO_3 glasses recorded with a magnification of 500 nm.

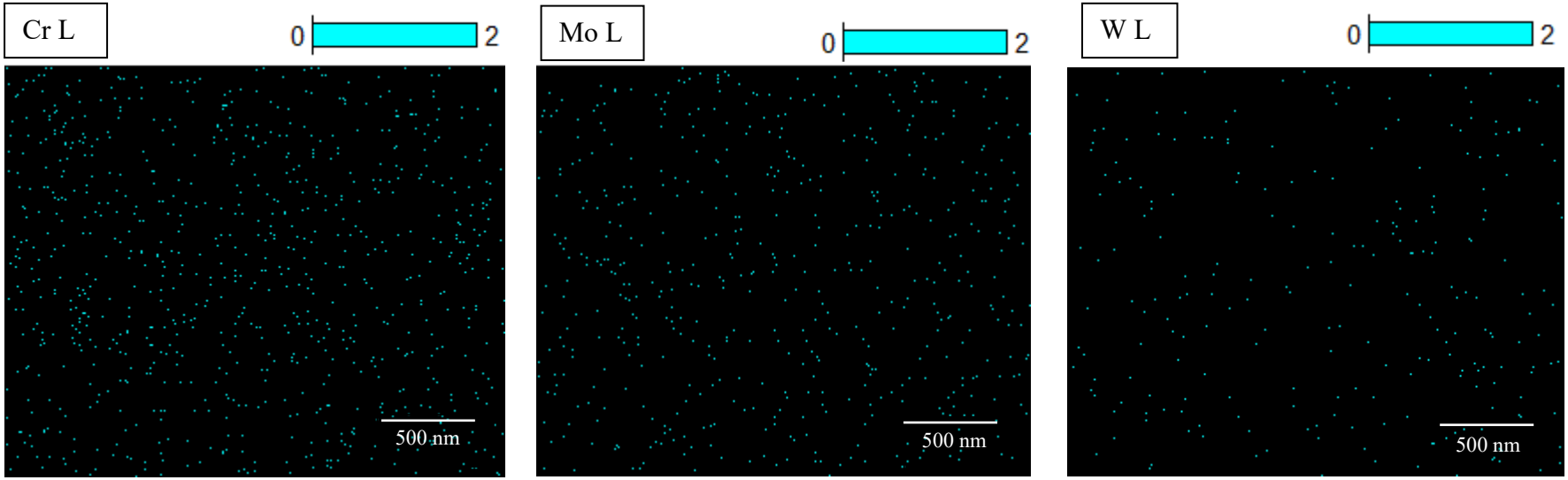

Figure 3. X-ray mappings of Cr, Mo, W elements in Li_2O-Al_2O_3-SiO_2 glasses.

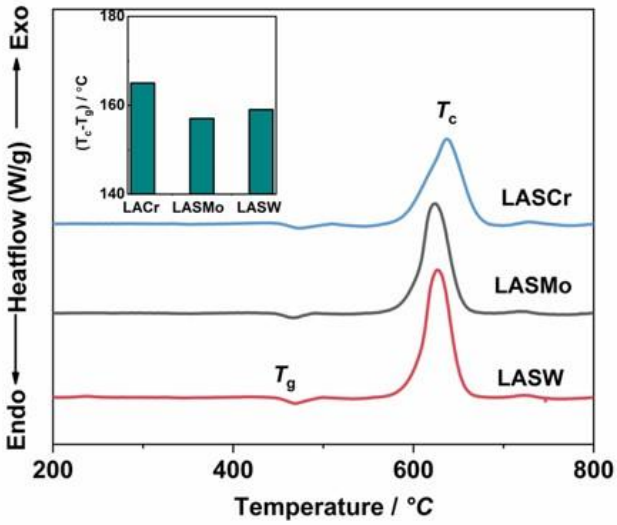

Figure 4. Traces of differential thermal analysis (DTA) of Li_2O-Al_2O_3-SiO_2:Cr_2O_3/MoO_3/WO_3 glasses, revealing glass transition (T_g) and crystallization temperatures. (Tc). Inset represents the values of (Tc–Tg) for the three glasses.

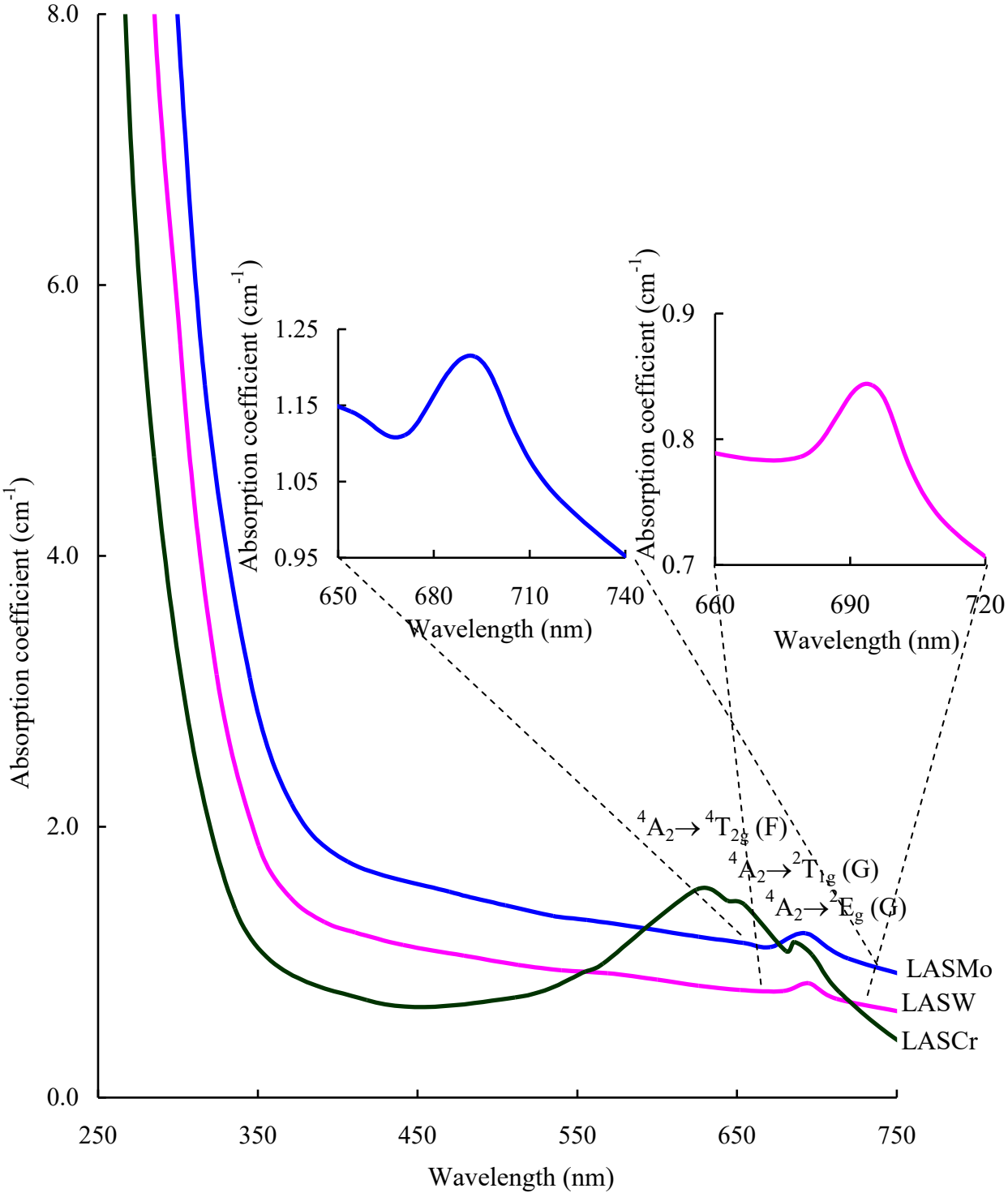

Figure 5a. Optical absorption spectra of Li_2O-Al_2O_3-SiO_2:Cr_2O_3/MoO_3/WO_3glasses recorded at ambient temperature with the indication of electronic transitions dopant ions. The insets highlight magnified views of peaks specific to LASMo and LASW glasses.

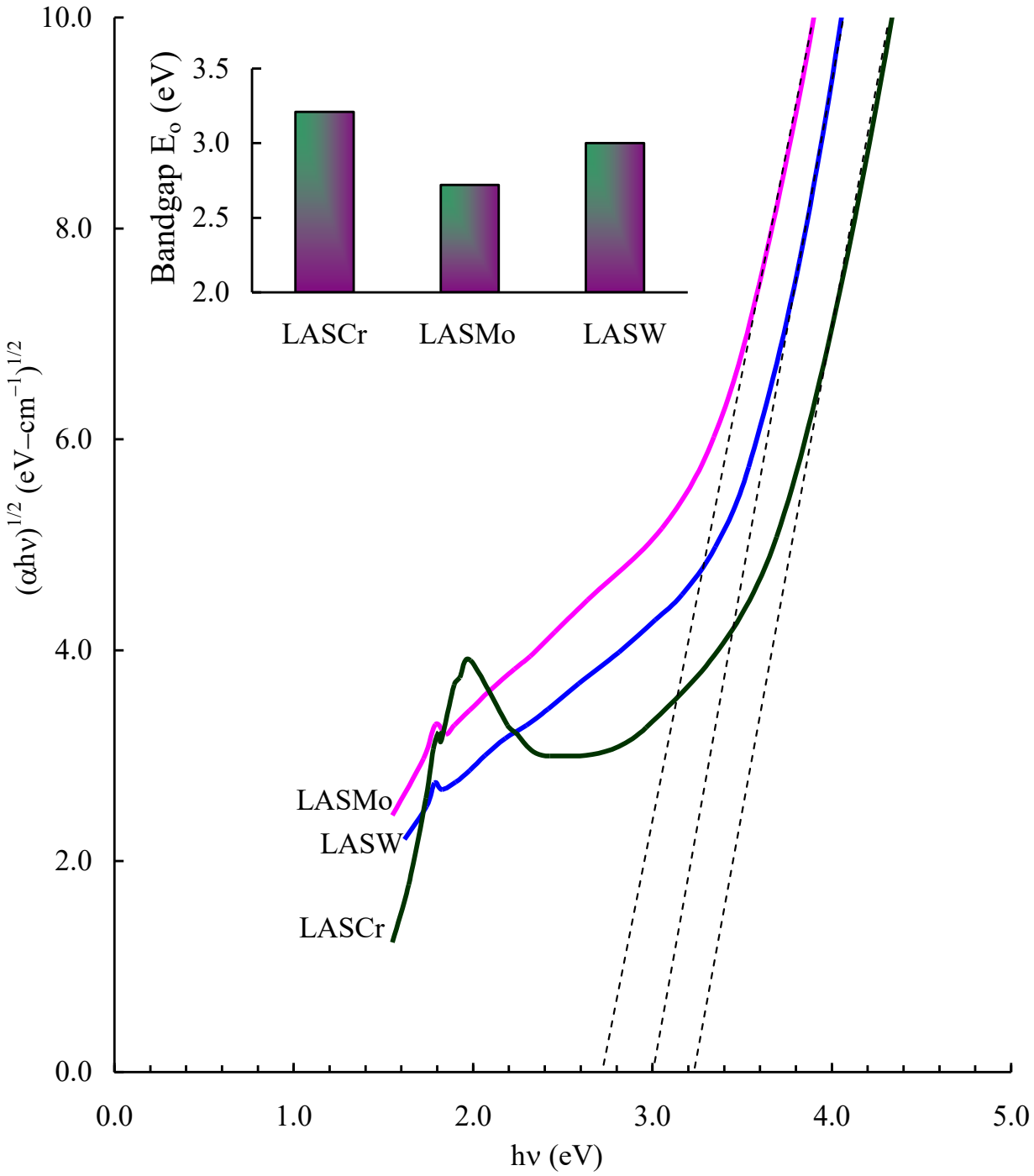

Figure 5b. The plots of $(\alpha h\nu)^{1/2}$ versus $h\nu$ (Tauc Plots) drawn to estimate the optical band gap energies (E_o) of Li_2O-Al_2O_3-SiO_2: Cr_2O_3/MoO_3/WO_3 glasses. The inset compares E_o values for all three studied glasses.

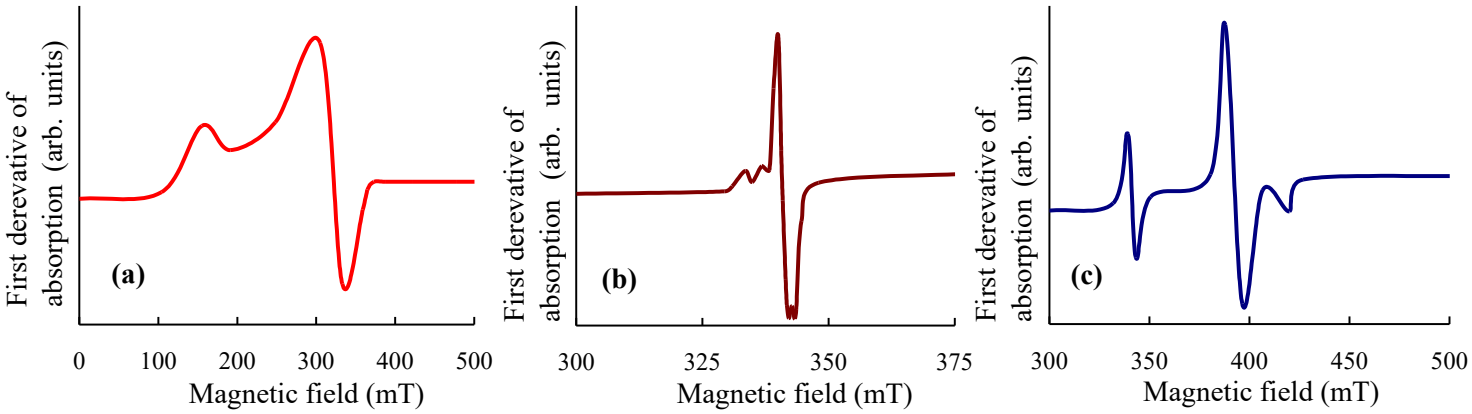

Figure 6. EPR spectra of Li_2O-Al_2O_3-SiO_2 glasses doped with **a** Cr_2O_3, **b** MoO_3 and **c** WO_3 recorded at ambient temperature

Figure 6.

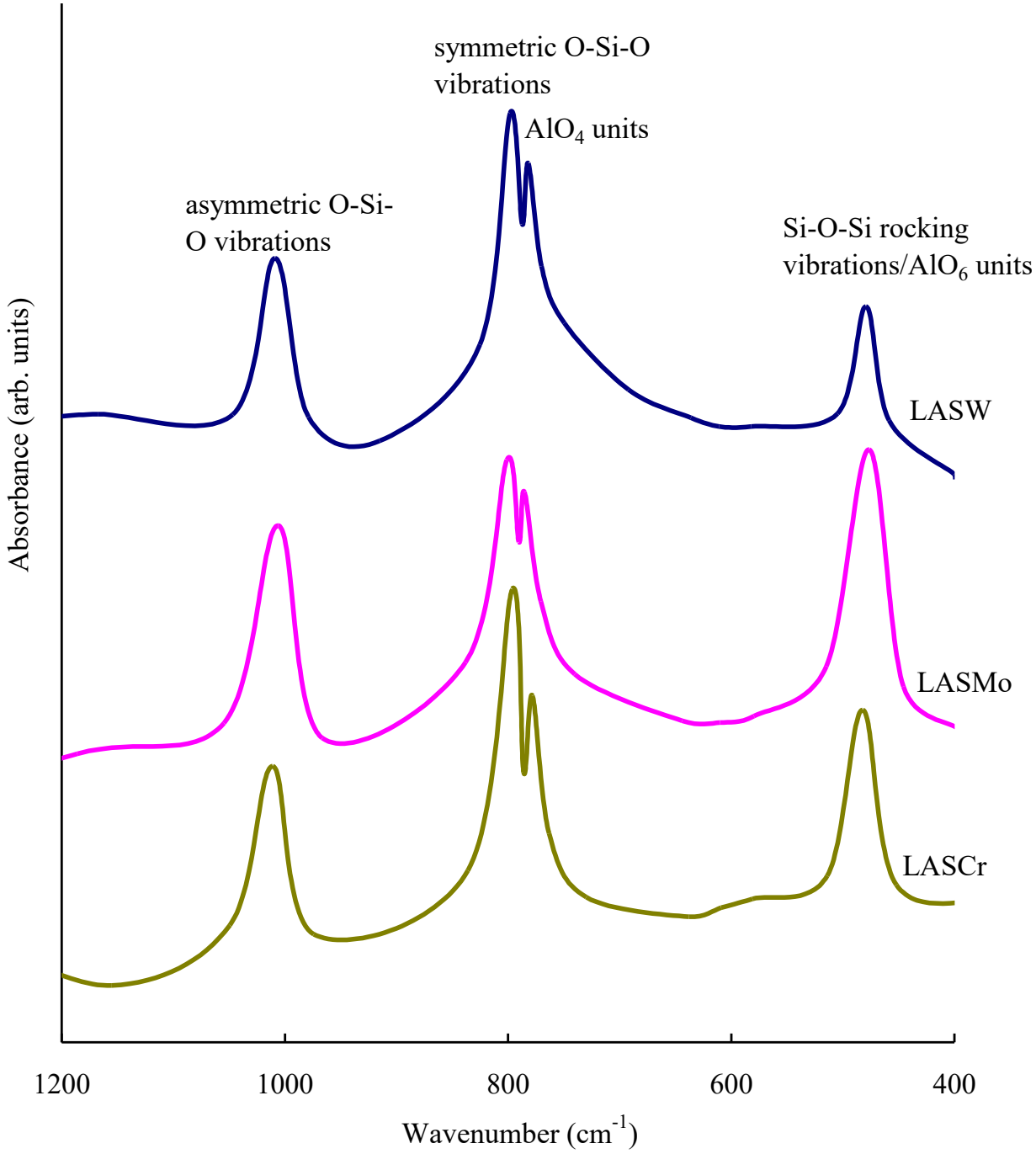

Figure 7. Fourier Transform Infrared (FT-IR) spectra of Li_2O-Al_2O_3-SiO_2:Cr_2O_3/MoO_3/WO_3 glasses recorded in attenuated total reflection (ATR) mode, providing information on vibrational bands of specific functional groups.

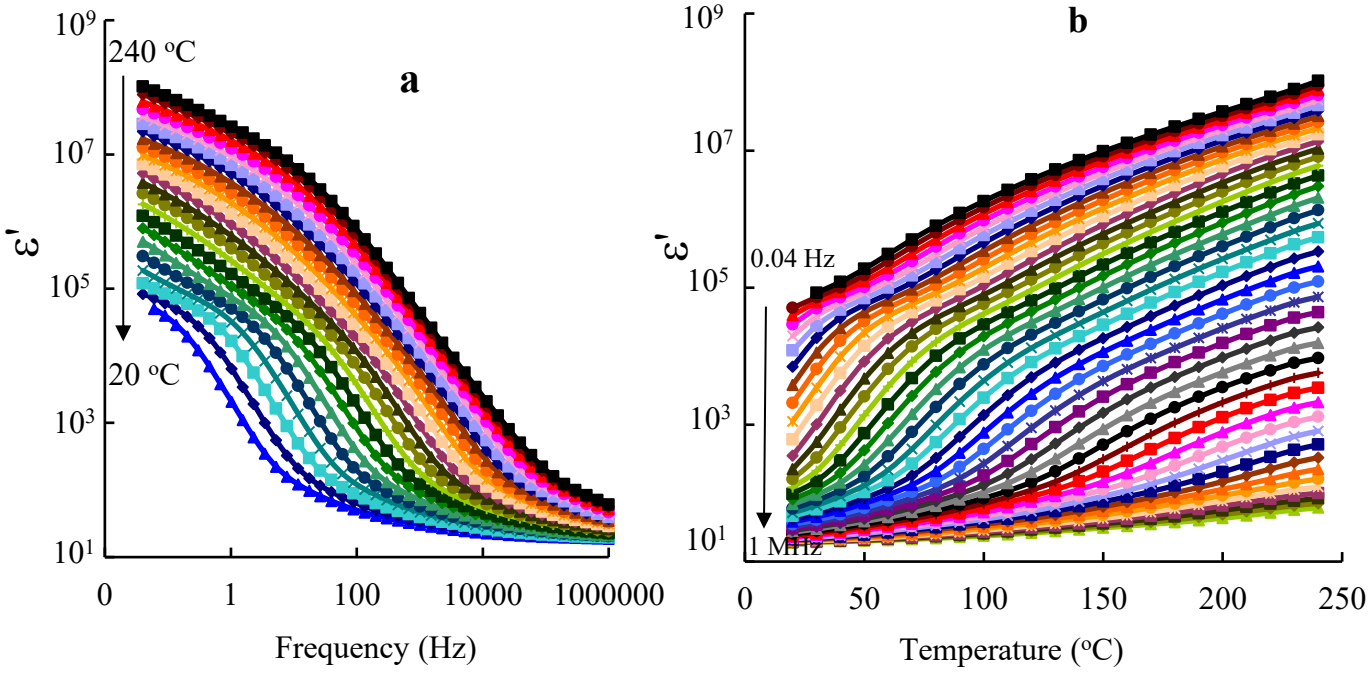

Figure 8. Variations of dielectric constant (ε') of LASCr glasses **a** with frequency measured at different temperatures and **b** with temperature measured at different frequencies illustrating the material's response to frequency of the applied electric field and temperature dependence of the material's dielectric properties.

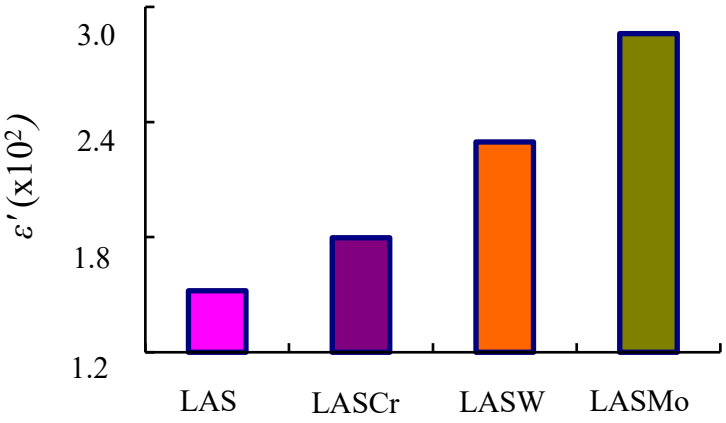

Figure 9. Comparison of dielectric constant at 100 °C and 1 kHz for Li_2O-Al_2O_3-SiO_2 glasses doped with 3.0 mol.% of Cr_2O_3, MoO_3, and WO_3, highlighting the influence of dopant type on dielectric behaviour.

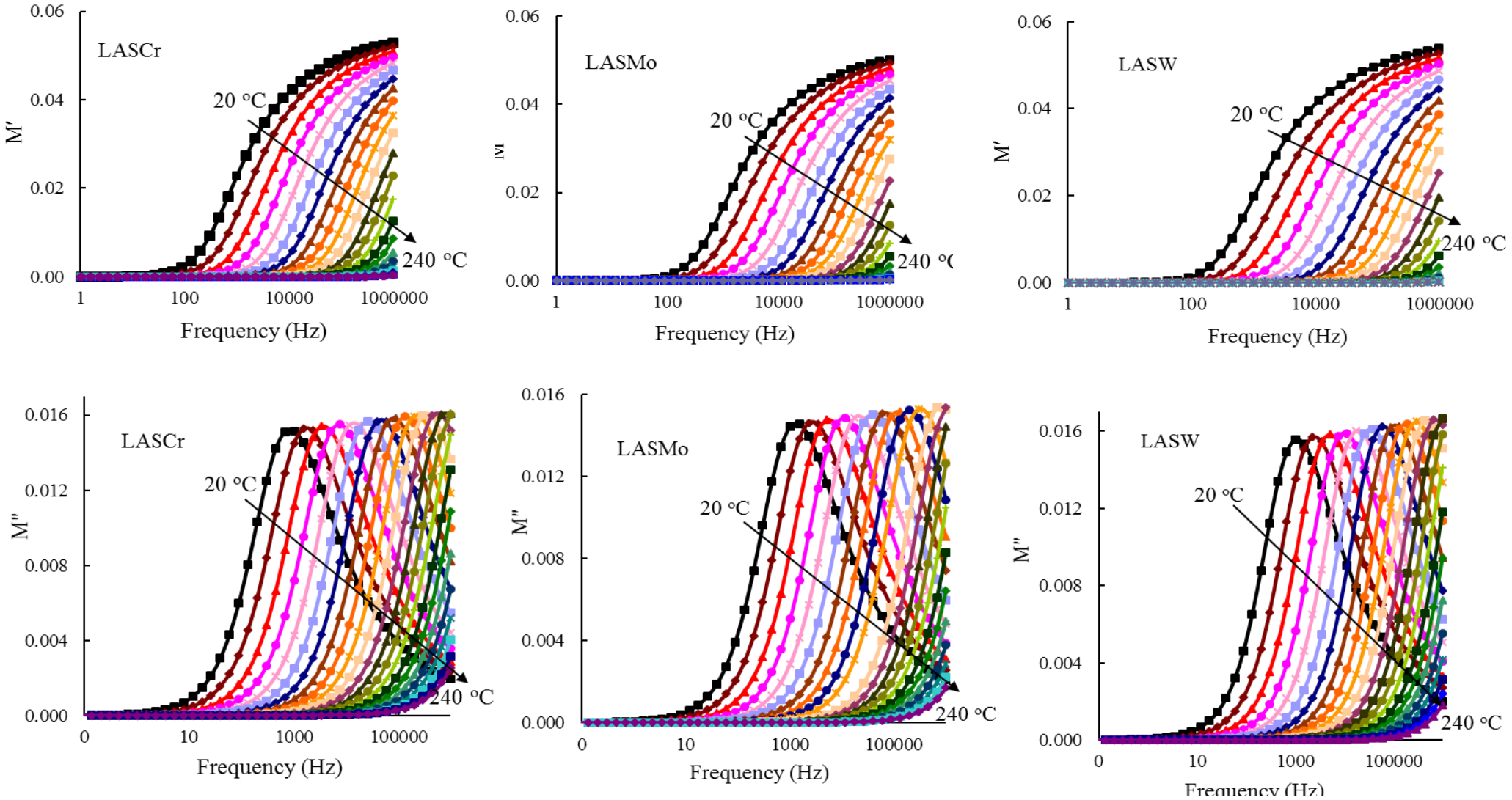

Figure10. Variations of real (M') and imaginary (M'') parts of electric moduli with frequency for LASCr, LASMo, and LASW glasses measured at different temperatures.

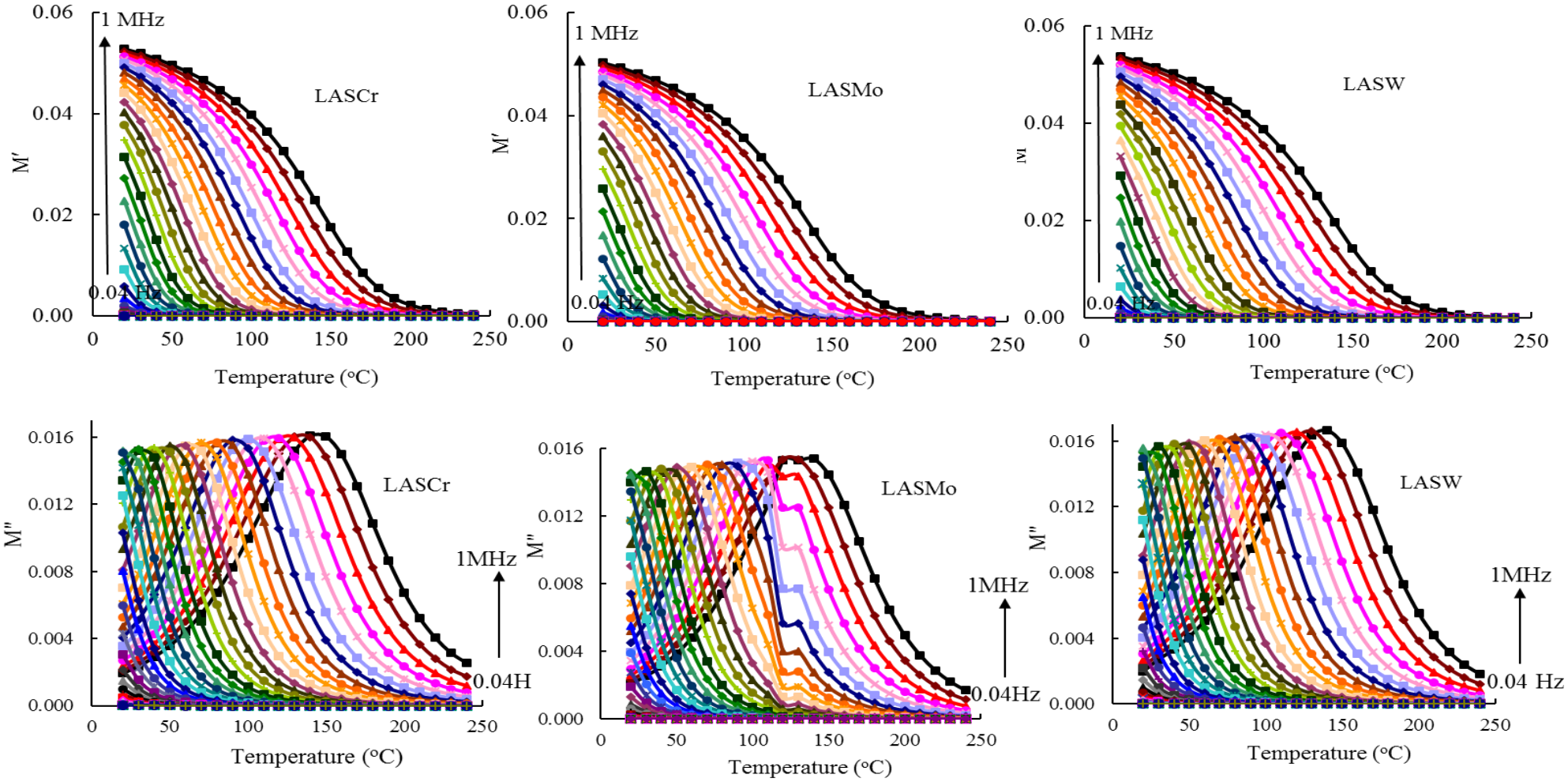

Figure 11. Variations of real and imaginary parts of electric moduli with temperature for Li_2O-Al_2O_3-SiO_2 glass doped with 3.0 mol.% of Cr_2O_3, MoO_3, and WO_3, revealing the combined effect of temperature and dopant on the material's response.

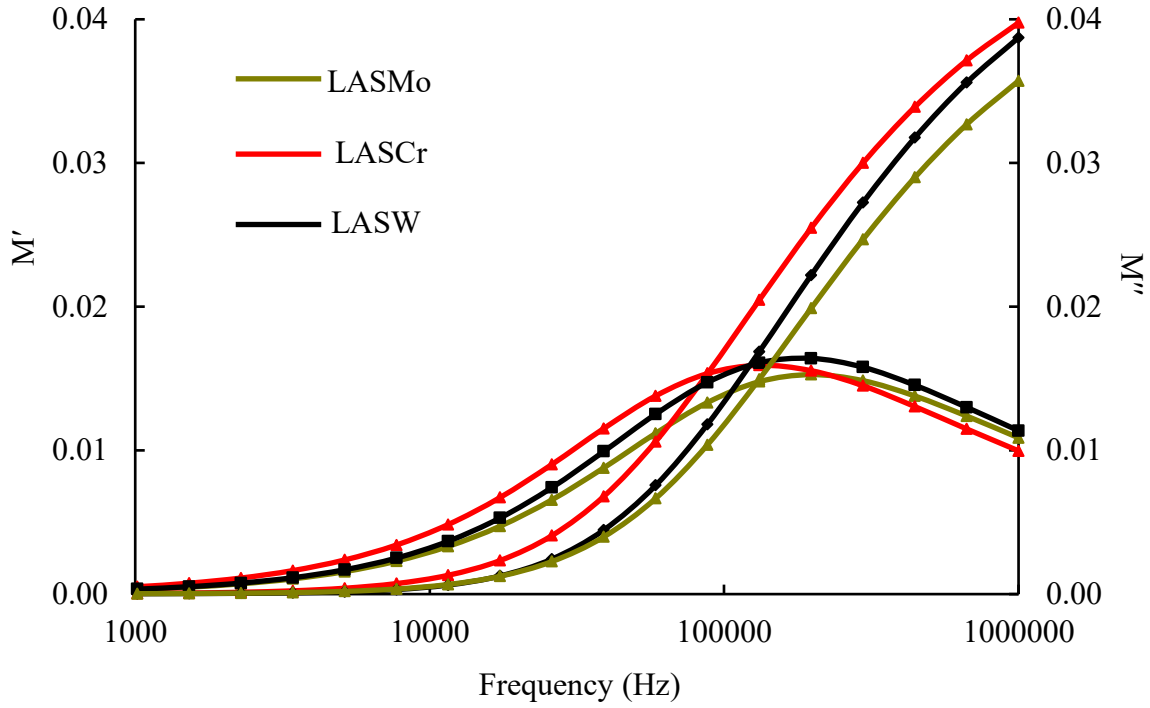

Figure 12. Plots of real and imaginary parts of electric moduli with frequency at 100 °C for LASCr, LASMo, and LASW glasses, used to estimate the relaxation time of each material.

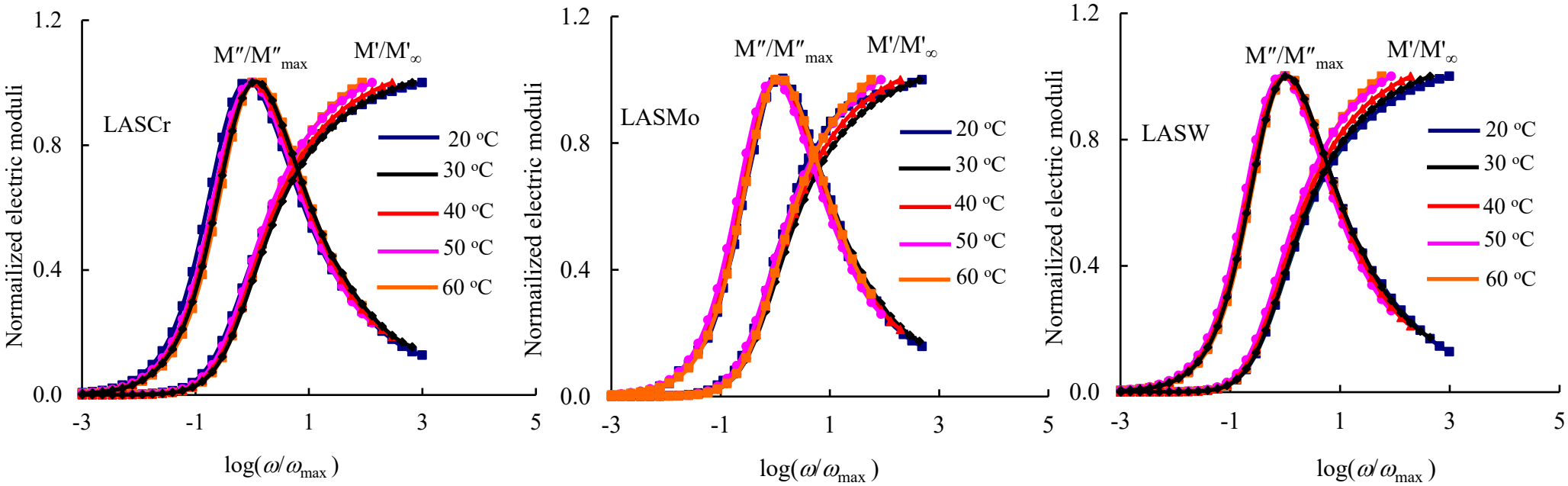

Figure 13. Scaling behavior of electric moduli with temperature for Li_2O-Al_2O_3-SiO_2: Cr_2O_3/MoO_3/WO_3 glasses between 20°C and 60°C, demonstrating the consistency of the response across different temperatures.

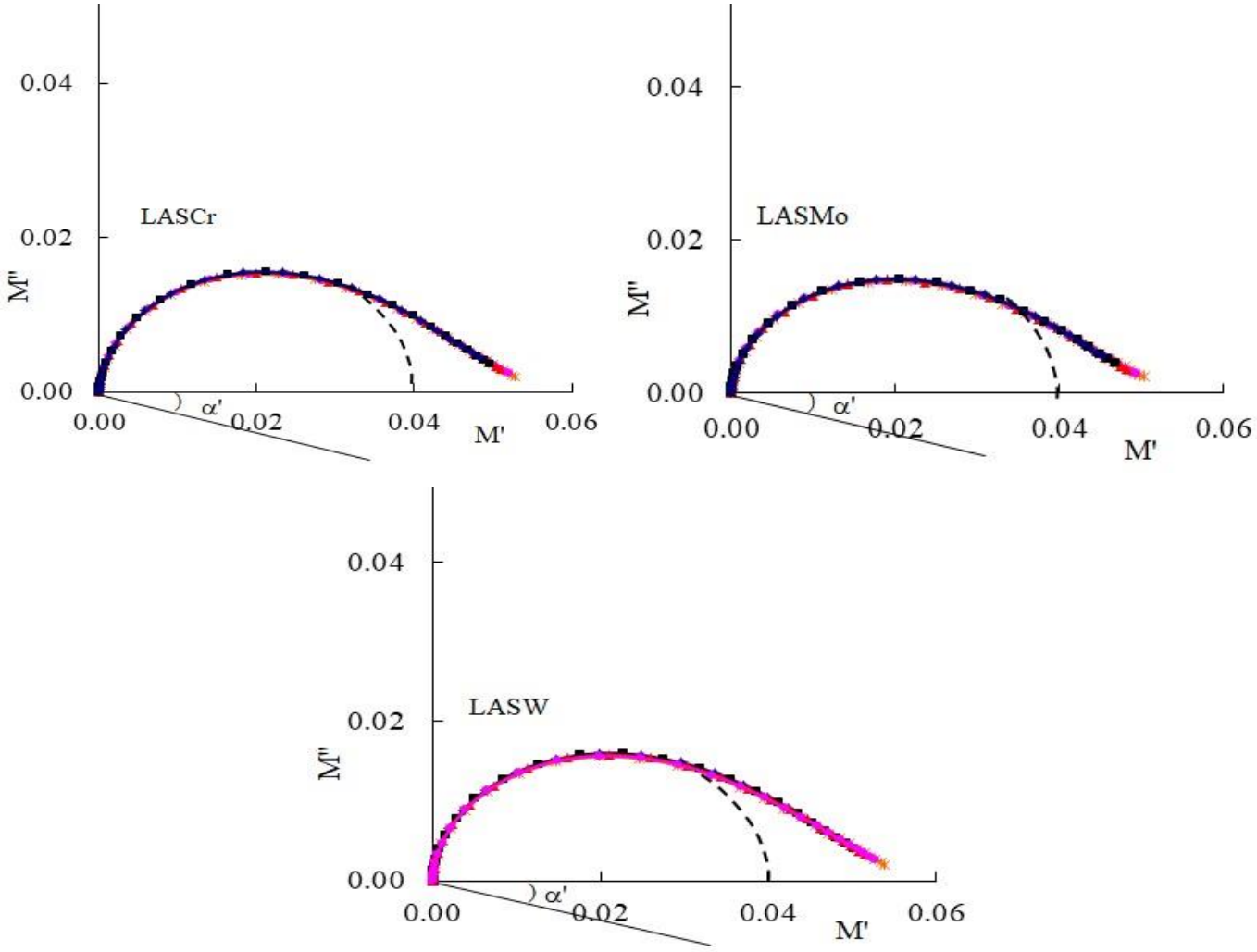

Figure 14. Cole-Cole plots for Li_2O-Al_2O_3-SiO_2 glass doped with Cr_2O_3, MoO_3, and WO_3 measured between 30°C and 100°C, visualizing the relaxation processes and conductivity mechanisms.

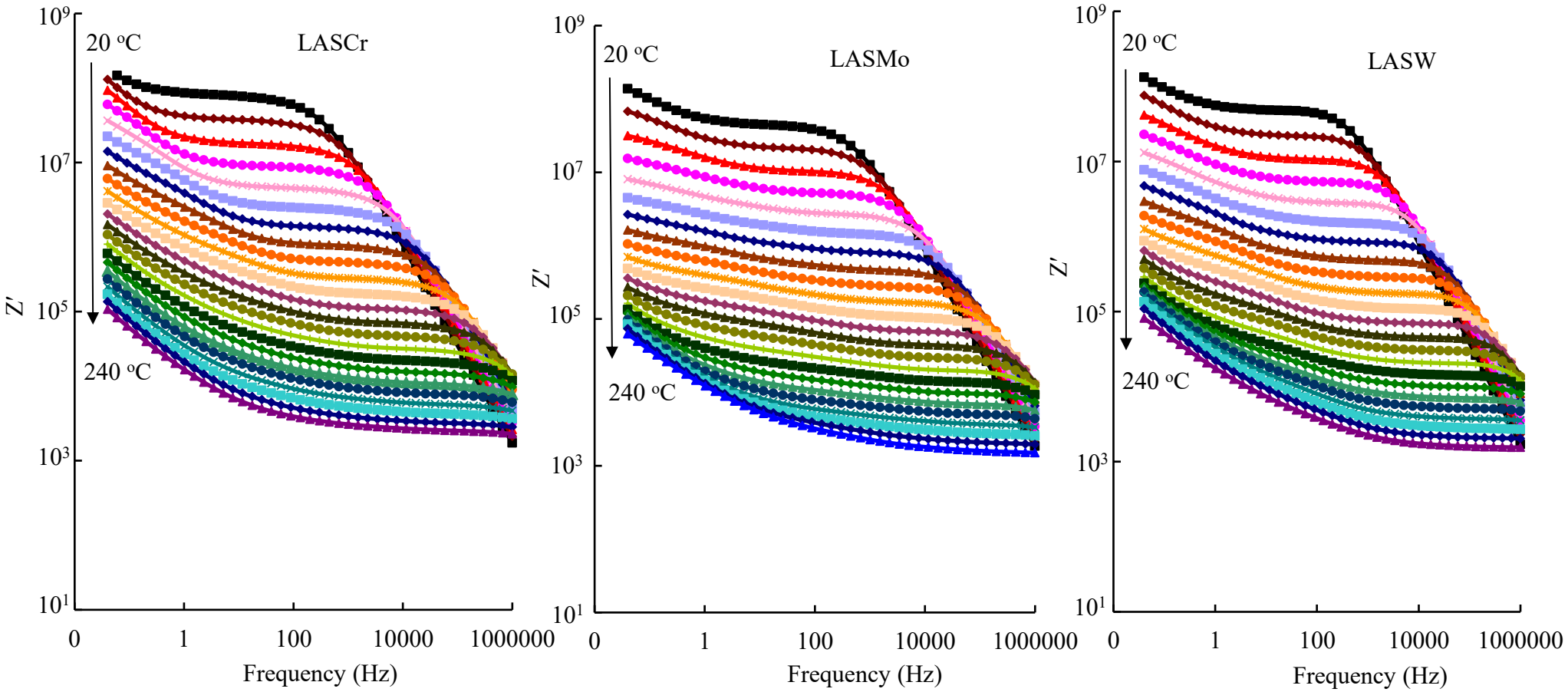

Figure 15. Variations of real part (*Z'*) of electrical impedance with frequency for Li_2O-Al_2O_3-SiO_2: Cr_2O_3/MoO_3/WO_3 glasses measured at different temperatures, indicating the resistive behavior of the materials.

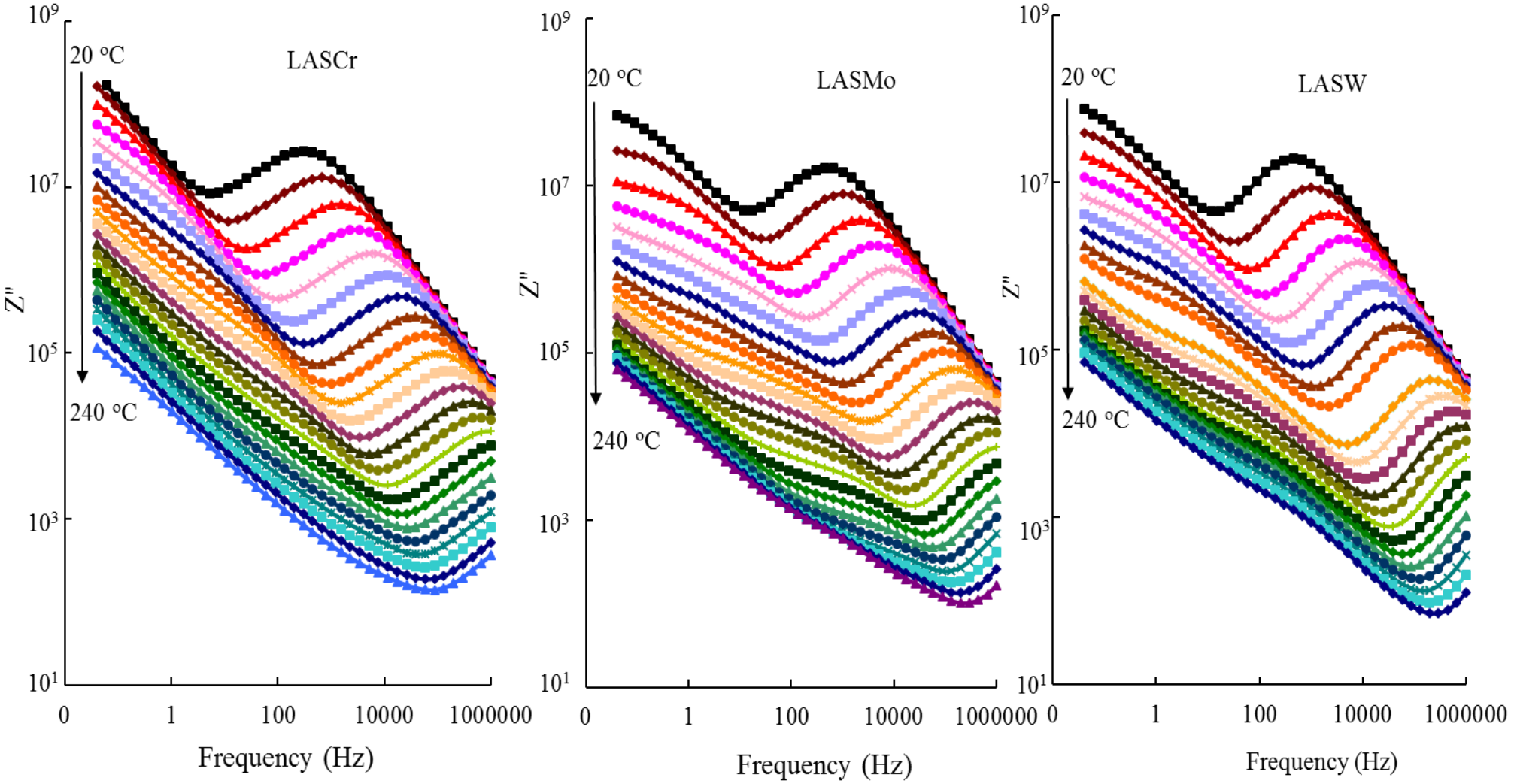

Figure 16. Variations of imaginary part (Z'') of electrical impedance with frequency for Li_2O-Al_2O_3-SiO_2:Cr_2O_3/MoO_3/WO_3 glasses measured at different temperatures, depicting the reactive behavior of the materials.

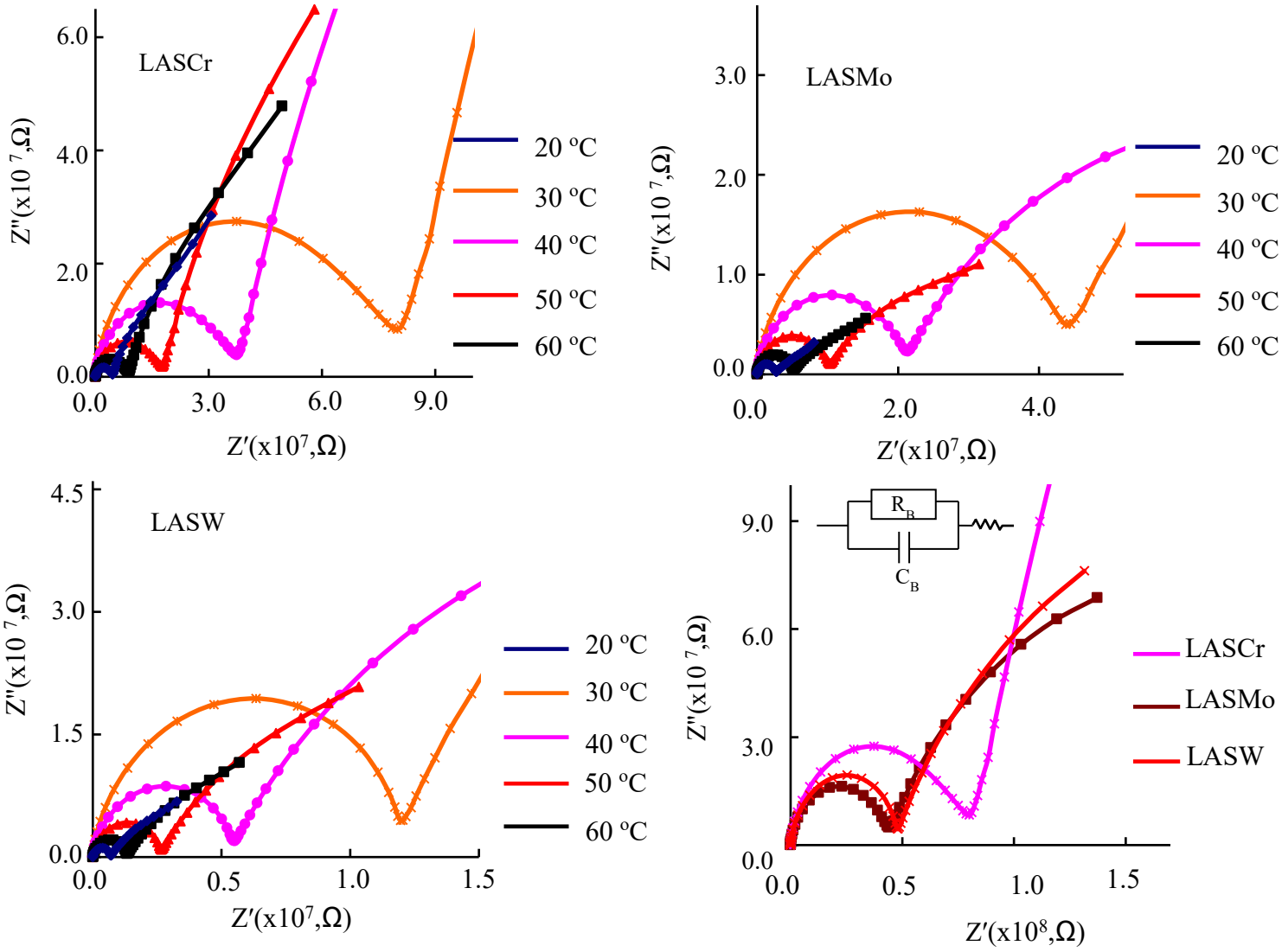

Figure17. Plots of Z'' vs Z' for LASCr, LASMo, and LASW glasses drawn in the temperature regions 20-60°C, along with equivalent circuit model, representing the distribution of resistive and capacitive components within the materials.

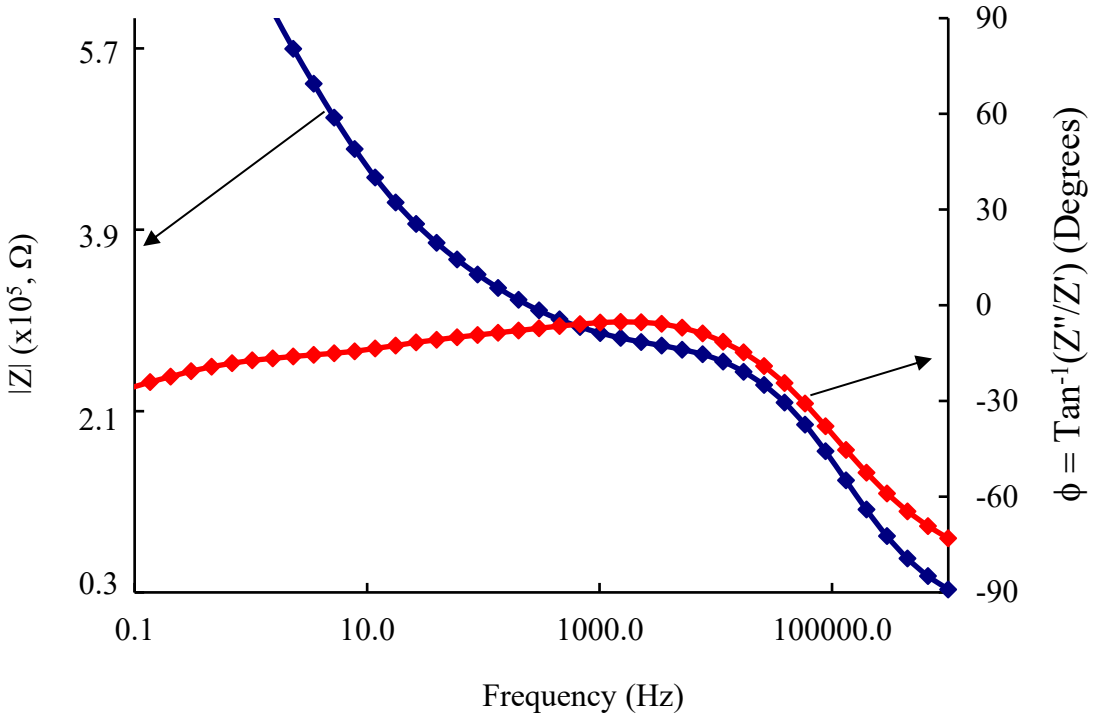

Figure 18. Bode plots of total impedance (|Z|) and phase angle (ϕ) for LASMo glass drawn at 100 °C, providing a comprehensive view of the frequency-dependent electrical response.

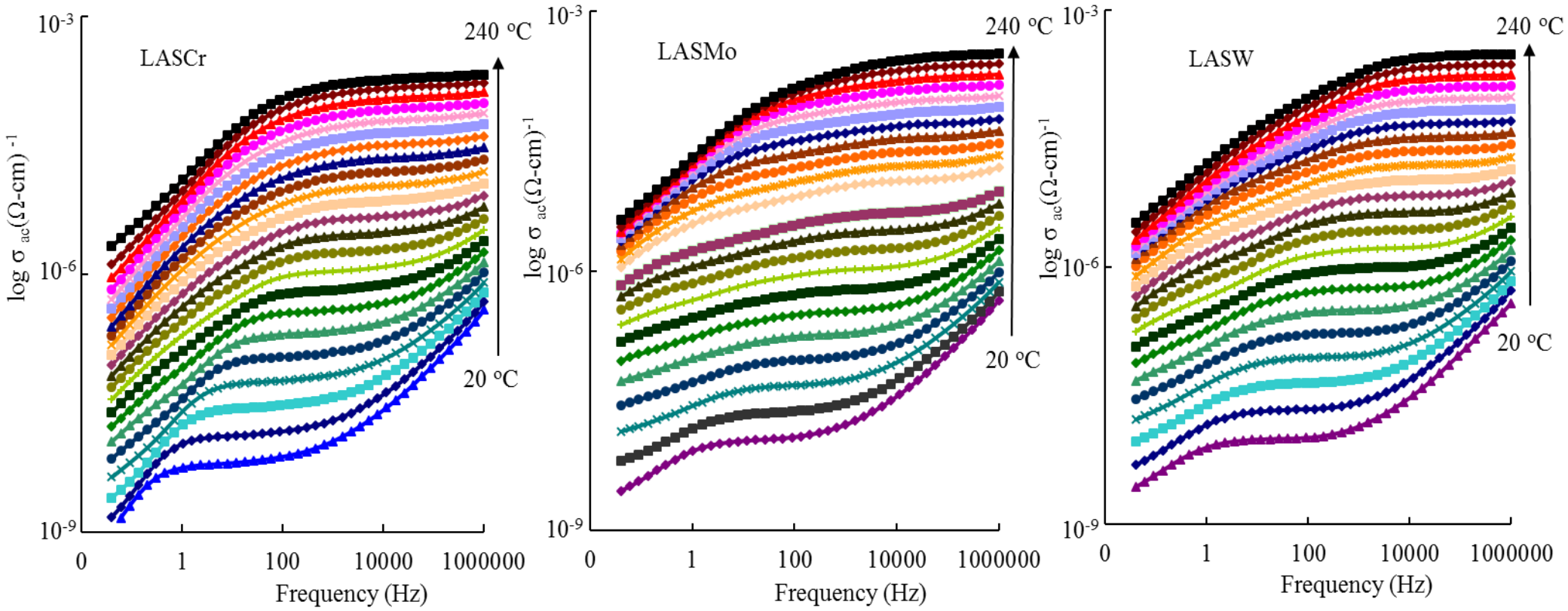

Figure 19a. Variation of log σ_{ac} with frequency (measured at different temperatures) of Li_2O-Al_2O_3-SiO_2:Cr_2O_3/MoO_3/WO_3 glasses doped with Cr_2O_3, WO_3 and MoO_3.

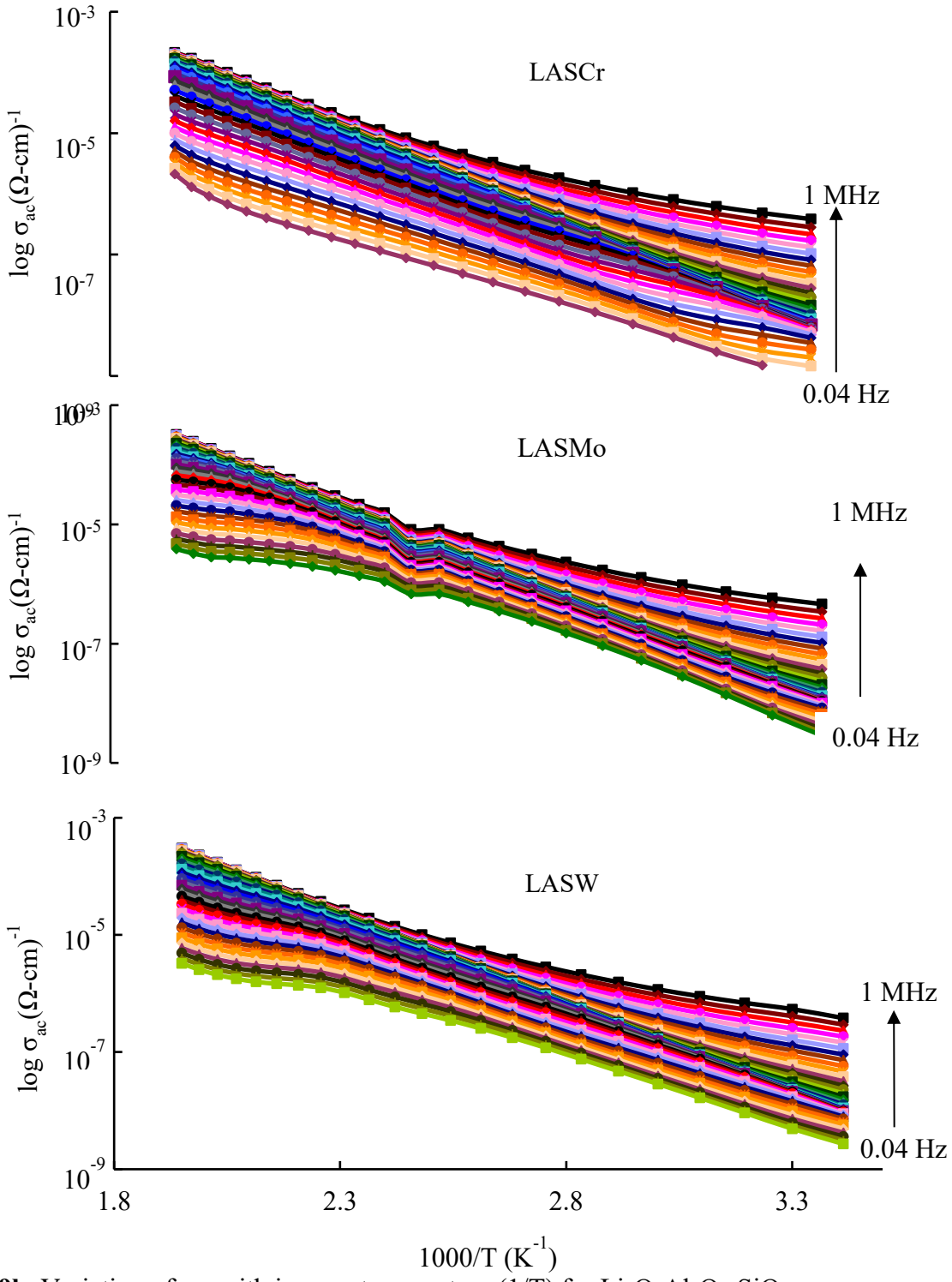

Figure 19b. Variation of σ_{ac} with inverse temperature (1/T) for Li_2O-Al_2O_3-SiO_2: Cr_2O_3/MoO_3/WO_3 glasses, drawn for evaluation of the activation energy required for charge conduction.

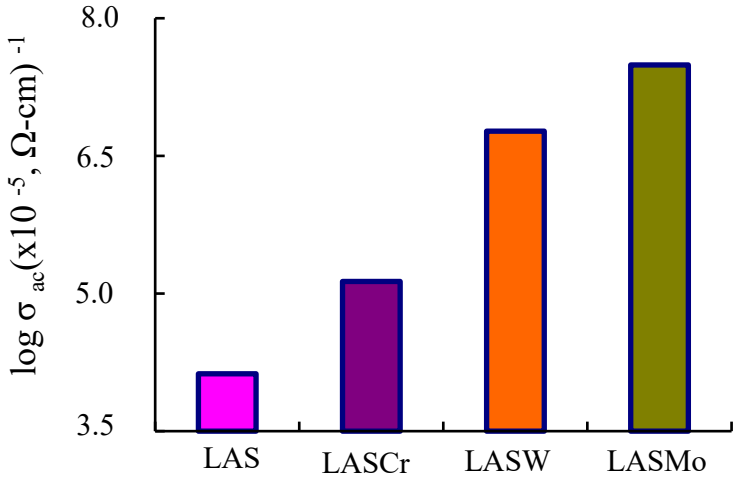

Figure 20. Comparison of σ_{ac} at 200 °C and 1 kHz for Li_2O-Al_2O_3-SiO_2 glasses doped with 3.0 mol.% of Cr_2O_3, WO_3, and MoO_3, highlighting the impact of dopant on conductivity.

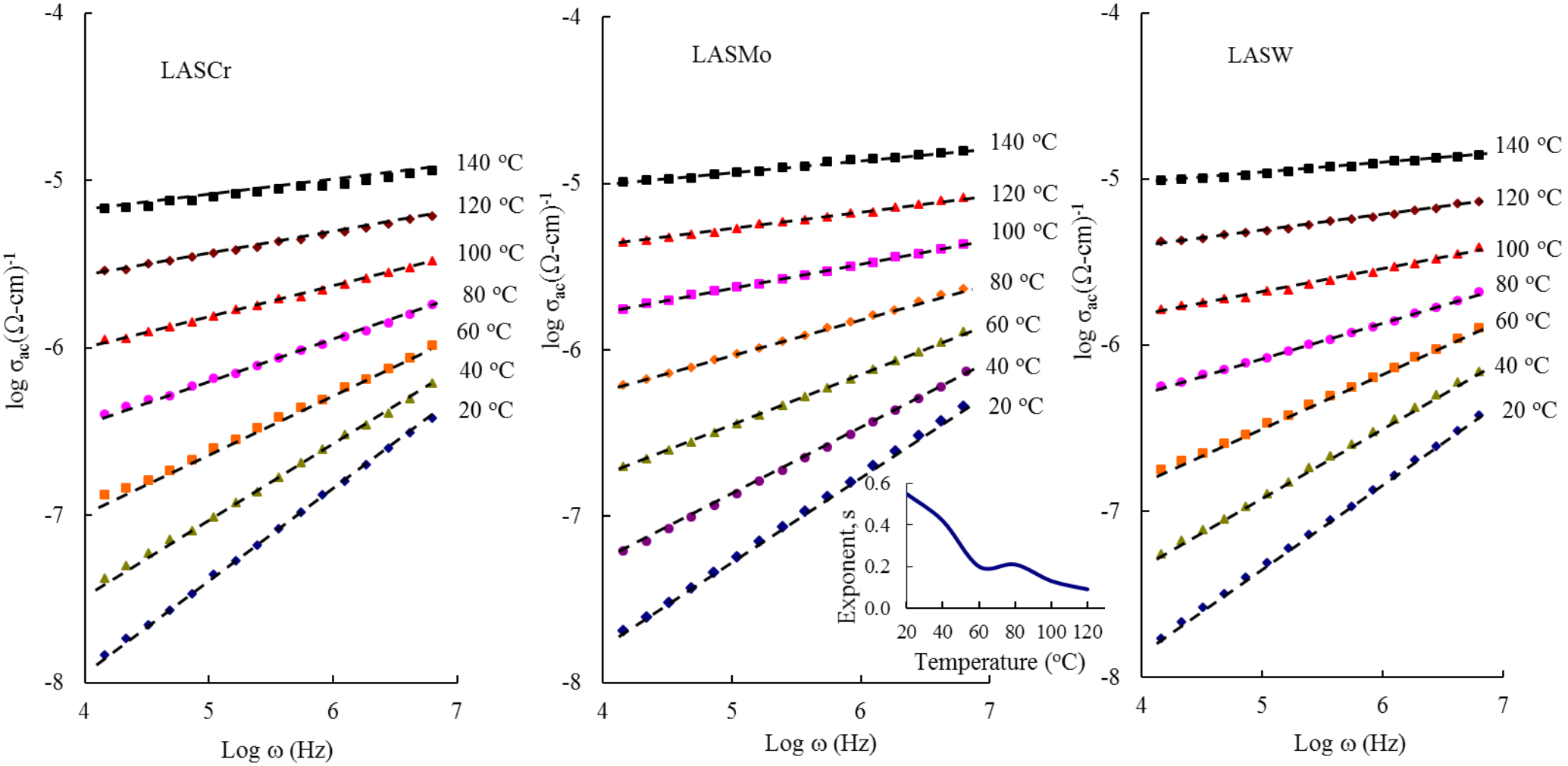

Figure 21. Variation of log σ_{ac} with log ω for Li_2O-Al_2O_3-SiO_2:Cr_2O_3/MoO_3/WO_3glasses, used to determine the exponent *s* in the power law relationship, indicating the conduction mechanism at different temperatures. The inset shows the temperature dependence of *s* for LASMo glass.